Characterization of Amino Acid Side Chain Dynamics in a Zinc-Finger Peptide Using ^{13}C NMR Spectroscopy and Time-Resolved Fluorescence Spectroscopy

Arthur G. Palmer, III,† Remo A. Hochstrasser, David P. Millar, Mark Rance, and Peter E. Wright*

Contribution from the Department of Molecular Biology, The Scripps Research Institute, La Jolla, California 92037

Received September 23, 1992

Abstract: Proton-detected ^{13}C NMR spectroscopy has been used to measure spin–lattice and spin–spin relaxation rate constants and the steady-state $\{^1H\}$-^{13}C nuclear Overhauser effect enhancements for the protonated aromatic carbon spins and for the methyl carbon spins in the zinc complex of a single zinc-finger peptide. Measurements were performed at 11.7 T for aromatic spins and at 7.0 and 11.7 T for methyl spins. Time-resolved fluorescence spectroscopy has been used to measure the polarization anisotropy decay for the single tyrosyl fluorophore in the peptide in the presence and absence of zinc. The NMR relaxation and fluorescence depolarization data are analyzed using a model-free formalism in which internal motions are characterized by order parameters and effective correlation times. Order parameters for Tyr and His aromatic moieties are similar to the order parameters for the corresponding backbone α carbon spins reported previously (Palmer, A. G.; Rance, M.; Wright, P. E. *J. Am. Chem. Soc.* **1991**, *113*, 4371–4380); thus, these aromatic side chains have little additional conformational freedom on picosecond to nanosecond time scales. In contrast, order parameters for Phe 10 indicate that the phenyl ring is more highly restricted than the backbone α carbon spin; thus, the order parameters reflect the packing of the Phe 10 side chain in the hydrophobic core of the molecule. Phenomenological spin–spin relaxation rate constants for the two His residues provide evidence that a chemical-exchange process occurs in the zinc-binding site of the peptide. Order parameters for the symmetry axes of the methyl groups are determined from the methyl C–H order parameters assuming tetrahedral geometry. In general, order parameters for the symmetry axes are smaller for residues with longer side chains; however, the order parameters for Leu 16 have nearly maximal values and reflect the packing of Leu 16 in the hydrophobic core of the peptide. The order parameters for the symmetry axes of the geminal methyl groups of Val and Leu residues are compared to order parameters obtained previously for the Val β and Leu γ methine carbon spins; the observed differences may reflect steric constraints on motions of the methyl and methine groups. The symmetry axis order parameter for Ala 15 is larger than unity and indicates that relaxation is mediated by motions with effective correlation times in excess of 100 ps. Analysis using specific models for internal motions of methyl groups suggests that the motion of this methyl group cannot be described simply by restricted rotational diffusion or three-site jump models. Order parameters measured by NMR and fluorescence spectroscopies for the tyrosyl ring in the zinc complex of the peptide are in good agreement; consequently, order parameters appear to be accurately determined by both experimental techniques. The overall rotational correlation time measured by fluorescence spectroscopy is 19% smaller than that measured by NMR spectroscopy. Fluorescence depolarization is faster in the absence of zinc and probably is dominated by large amplitude local motions of the unfolded peptide.

Introduction

Nuclear magnetic spin relaxation and fluorescence depolarization are coupled to stochastic overall and internal motions of molecules in solution. Consequently, nuclear magnetic resonance (NMR)[1,2] and fluorescence spectroscopies[3,4] are powerful techniques for experimental investigation of dynamics at individual sites in molecules. Characterization of motional phenomena in biological macromolecules is critical for a detailed biophysical understanding of function and complements determination of the time-averaged three-dimensional structures by X-ray crystallography and NMR spectroscopy.

Direct measurements of ^{13}C and ^{15}N spin relaxation in biological macromolecules are hindered by the small gyromagnetic ratios of these nuclei and by the limited resolution of one-dimensional NMR techniques. Proton-detected two-dimensional heteronuclear NMR spectroscopy provides significant improvements in sensitivity and resolution and has rejuvenated the study of ^{13}C and ^{15}N spin relaxation in biological macromolecules.[5–8] Characterization of ^{13}C relaxation is particularly useful for investigation of dynamics in peptides and proteins because carbon atoms are distributed along the amino acid backbones and throughout side chains;[9–12] nonetheless, investigations of backbone dynamics of proteins using ^{15}N NMR spectroscopy have been more common because of the availability of isotopically enriched species.[13–20]

† Present address: Department of Biochemistry and Molecular Biophysics, College of Physicians and Surgeons, Columbia University, New York, NY 10032.

(1) London, R. E. *Methods Enzymol.* **1989**, *176*, 358–375.
(2) Williams, R. J. P. *Eur. J. Biochem.* **1989**, *183*, 479–497.
(3) Beechem, J. M.; Brand, L. *Annu. Rev. Biochem.* **1985**, *54*, 43–71.
(4) Bucci, E.; Steiner, R. F. *Biophys. Chem.* **1988**, *30*, 199–224.
(5) Kay, L. E.; Jue, T. L.; Bangerter, B.; Demou, P. C. *J. Magn. Reson.* **1987**, *73*, 558–564.
(6) Sklenar, V.; Torchia, D.; Bax, A. *J. Magn. Reson.* **1987**, *73*, 375–379.
(7) Nirmala, N. R.; Wagner, G. *J. Am. Chem. Soc.* **1988**, *110*, 7557–7558.
(8) Nirmala, N. R.; Wagner, G. *J. Magn. Reson.* **1989**, *82*, 659–661.
(9) Dellwo, M. J.; Wand, A. J. *J. Am. Chem. Soc.* **1989**, *111*, 4571–4578.
(10) Palmer, A. G.; Rance, M.; Wright, P. E. *J. Am. Chem. Soc.* **1991**, *113*, 4371–4380.
(11) Kelsh, L. P.; Ellena, J. F.; Cafiso, D. S. *Biochemistry* **1992**, *31*, 5136–5144.
(12) Nicholson, L. K.; Kay, L. E.; Baldisseri, D. M.; Arango, J.; Young, P. E.; Torchia, D. A. *Biochemistry* **1992**, *31*, 5253–5263.
(13) Kay, L. E.; Torchia, D. A.; Bax, A. *Biochemistry* **1989**, *28*, 8972–8979.
(14) Clore, G. M.; Driscoll, P. C.; Wingfield, P. T.; Gronenborn, A. M. *Biochemistry* **1990**, *29*, 7387–7401.
(15) Barbato, G.; Ikura, M.; Kay, L. E.; Pastor, R. W.; Bax, A. *Biochemistry* **1992**, *31*, 5269–5278.

0002-7863/93/1515-6333$04.00/0

Time-resolved decay of the polarization anisotropy of fluorescence emission has been used extensively to examine motional properties of intrinsic and extrinsic fluorescent probes in proteins.[3,4] Fluorescence spectroscopy is more sensitive than NMR spectroscopy and directly monitors dynamic processes on picosecond and nanosecond time scales; however, the number of molecular sites available for investigation is more limited. Relatively few investigations of intrinsic fluorescence in proteins have utilized the Tyr fluorophore,[21-23] because Tyr fluorescence usually is quenched by nearby Trp residues. In addition, few investigations have been reported that compare motional parameters obtained from NMR and fluorescence spectroscopies.[24,25]

The intramolecular dynamics of the zinc complex of a 25 amino acid zinc-finger peptide, Xfin-31, have been characterized previously for the backbone C^{α} spins and for the side chain Val C^{β} and Leu C^{γ} spins.[10] In the present study, recently developed techniques for proton-detected ^{13}C relaxation measurements are used to quantify relaxation parameters for the protonated carbons of the Tyr, Phe, and His aromatic moieties and the terminal methyl carbon spins of the Ala, Val, and Leu residues. Time-resolved fluorescence spectroscopy is used to measure the polarization anisotropy decay of the single Tyr fluorophore in Xfin-31 in the presence and absence of zinc. NMR and fluorescence results are interpreted using both model-free methods and specific motional models for internal dynamics. A comparison of the experimental NMR results with the results of molecular dynamics simulations is reported elsewhere.[26]

Theory

NMR spin relaxation parameters are measured using two-dimensional proton-detected analogs of the inversion–recovery,[27] Carr–Purcell–Meiboom–Gill (CPMG),[28,29] and steady-state nuclear Overhauser effect (NOE) experiments.[30] Ignoring cross-correlation between dipolar and chemical shift anisotropy (CSA) relaxation mechanisms[31] and cross-correlation between methyl bond vectors,[32] the spin–lattice relaxation rate constant, spin–spin relaxation rate constant, and steady-state $\{^1H\}$–^{13}C NOE enhancement are given by, respectively,[33,34]

$$R_1 = n_p D^2/_4\{J(\omega_H-\omega_C) + 3J(\omega_C) + 6J(\omega_H+\omega_C)\} + C^2J(\omega_C) \quad (1)$$

$$R_2 = n_p D^2/_8\{4J(0) + J(\omega_H-\omega_C) + 3J(\omega_C) + 6J(\omega_H) + 6J(\omega_H+\omega_C)\} + C^2/_6\{4J(0) + 3J(\omega_C)\} + R_a \quad (2)$$

$$\eta = n_p D^2\gamma_H/(4\gamma_C)\{6J(\omega_H+\omega_C) - J(\omega_H-\omega_C)\}/R_1 \quad (3)$$

in which

$$D = (\mu_0/4\pi)\hbar\gamma_H\gamma_C/r_{CH}^3 \quad (4)$$

$$C = \omega_C\Delta\sigma/\sqrt{3} \quad (5)$$

n_p is the number of protons directly attached to the carbon atom of interest; γ_H and γ_C are the gyromagnetic ratios of the proton and ^{13}C spins, respectively; r_{CH} is the length of the C–H bond vector; ω_H and ω_C are the Larmor frequencies of the ^1H and ^{13}C spins, respectively; $\Delta\sigma$ is the chemical shift anisotropy; $\hbar$ is Planck's constant divided by 2π; and μ_0 is the permittivity of free space. For an axially symmetric chemical shift tensor with parallel and perpendicular components denoted $\sigma_\parallel$ and $\sigma_\perp$, respectively, $\Delta\sigma = \sigma_\parallel - \sigma_\perp$. In eq 2, R_a is the systematic contribution to R_2 from processes, such as chemical exchange, that lead to dephasing of the ^{13}C magnetization during the CPMG pulse train; R_a is significant only if $k\tau > 1$, in which k is the rate constant of the dephasing mechanism and 2τ is the pulse spacing in the CPMG sequence.[35]

The auto-spectral density function, $J(\omega)$, is the Fourier transform of the orientational autocorrelation function, $C(\tau)$,

$$J(\omega) = 2\int_0^\infty C(\tau)\cos\omega\tau\,d\tau \quad (6)$$

with

$$C(\tau) = \langle Y_2^0[\Omega(0)]Y_2^0[\Omega(\tau)]\rangle = {}^1/_5\langle P_2[\mu_r(0)\cdot\mu_r(\tau)]\rangle \quad (7)$$

in which $Y_2^0[\Omega(t)]$ is a modified spherical harmonic function,[36] $P_2(x)$ is the second Legendre polynomial, $\Omega(t)$ are the polar angles specifying the orientation in the laboratory frame of a unit vector, $\mu_r(t)$, that is defined by the relevant relaxation mechanism, and $\langle\ \rangle$ indicates an ensemble average. For dipolar relaxation, $\mu_r(t)$ points along the C–H bond; for CSA relaxation by a symmetric chemical shift tensor, $\mu_r(t)$ points along the principal axis of the tensor.[34]

In a time-resolved fluorescence depolarization experiment, fluorophores in the sample are excited by a laser pulse that propagates along the y-axis and is polarized in the z-direction, in the laboratory reference frame. The intensities of the components of the emitted fluorescence that are polarized parallel, $I_\parallel(t)$, and perpendicular, $I_\perp(t)$, to the z-axis are measured in the x-direction as functions of the time following the pulse, t. The fluorescence polarization anisotropy is given by

$$r(t) = [I_\parallel(t) - I_\perp(t)]/[I_\parallel(t) + 2I_\perp(t)] \quad (8)$$

If unit vectors along the directions of the absorption and emission dipole transition moments, $\mu_a(t)$ and $\mu_e(t)$, respectively, are parallel, or if the fluorophore is axially symmetric about $\mu_e(t)$, then

$$r(t) = {}^2/_5P_2(\cos\lambda)\langle P_2[\mu_e(0)\cdot\mu_e(t)]\rangle = r_0\langle P_2[\mu_e(0)\cdot\mu_e(t)]\rangle \quad (9)$$

in which λ is the constant angle between $\mu_a(t)$ and $\mu_e(t)$, and r_0 is the limiting polarization anisotropy.[37] As shown by eq 9, $r_0 \leq 0.4$, and the equality is satisfied if μ_a and μ_e are parallel.

The formal correspondence between NMR spin relaxation and fluorescence depolarization is indicated by the right-hand sides of eqs 7 and 9: both phenomena depend upon molecular motions through an autocorrelation function of the form $\langle P_2[\mu(0)\cdot\mu(\tau)]\rangle$. In the following, the motions of a unit vector $\mu(t)$ attached to an

(16) Kördel, J.; Skelton, N. J.; Akke, M.; Palmer, A. G.; Chazin, W. J. *Biochemistry* **1992**, *31*, 4856–4866.
(17) Peng, J. W.; Wagner, G. *Biochemistry* **1992**, *31*, 8571–8586.
(18) Schneider, D. M.; Dellwo, M. J.; Wand, A. J. *Biochemistry* **1992**, *31*, 3645–3652.
(19) Stone, M. J.; Fairbrother, W. J.; Palmer, A. G.; Reizer, J.; Saier, M. H.; Wright, P. E. *Biochemistry* **1992**, *31*, 4394–4406.
(20) Stone, M. J.; Chandrasekhar, K.; Holmgren, A.; Wright, P. E.; Dyson, H. J. *Biochemistry* **1993**, *32*, 426–435.
(21) Härd, T.; Hsu, V.; Sayre, M. H.; Geiduschek, E. P.; Appelt, K.; Kearns, D. R. *Biochemistry* **1989**, *28*, 396–406.
(22) Lakowicz, J. R.; Laczko, G.; Gryczynski, I. *Biochemistry* **1987**, *26*, 82–90.
(23) Rigler, R.; Roslund, J.; Forsén, S. *Eur. J. Biochem.* **1990**, *188*, 541–545.
(24) Weaver, A. J.; Kemple, M. D.; Prendergast, F. G. *Biophys. J.* **1988**, *54*, 1–15.
(25) Weaver, A. J.; Kemple, M. D.; Prendergast, F. G. *Biochemistry* **1989**, *28*, 8614–8623.
(26) Palmer, A. G.; Case, D. A. *J. Am. Chem. Soc.* **1992**, *114*, 9059–9067.
(27) Vold, R. L.; Waugh, J. S.; Klein, M. P.; Phelps, D. E. *J. Chem. Phys.* **1968**, *48*, 3831–3832.
(28) Carr, H. Y.; Purcell, E. M. *Phys. Rev.* **1954**, *94*, 630–638.
(29) Meiboom, S.; Gill, D. *Rev. Sci. Instrum.* **1958**, *29*, 688–691.
(30) Noggle, J. H.; Shirmer, R. E. *The Nuclear Overhauser Effect: Chemical Applications*; Academic Press: New York, 1971.
(31) Goldman, M. *J. Magn. Reson.* **1984**, *60*, 437–452.
(32) Werbelow, L. G.; Grant, D. M. *Adv. Magn. Reson.* **1977**, *9*, 189–299.
(33) Abragam, A. *Principles of Nuclear Magnetism*; Clarendon Press: Oxford, U.K. 1961.
(34) Lipari, G.; Szabo, A. *J. Am. Chem. Soc.* **1982**, *104*, 4546–4559.
(35) Bloom, M.; Reeves, L. W.; Wells, E. J. *J. Chem. Phys.* **1965**, *42*, 1615–1624.
(36) Brink, D. M.; Satchler, G. R. *Angular Momentum*; Clarendon Press: Oxford, U.K. 1968.
(37) Lipari, G.; Szabo, A. *Biophys. J.* **1980**, *30*, 489–506.

amino acid side chain are described by time-dependent coordinate transformations first from the laboratory frame to a fixed molecular reference frame M and then from frame M to an internal frame D in which the orientation of the vector is constant. Assuming that overall rotational motion of the molecule is isotropic and independent of internal motions, the autocorrelation function is given by

$$G(\tau) = \langle P_2[\mu(0)\cdot\mu(\tau)]\rangle = \exp[-\tau/\tau_m] \sum_{a=-2}^{2}\sum_{b=-2}^{2}\sum_{b'=-2}^{2} \times \langle \mathbf{D}_{a,b}{}^{2*}[\Omega_{MD}(0)]\mathbf{D}_{a,b'}{}^{2}[\Omega_{MD}(\tau)]\rangle \times Y_2{}^{b*}[\beta_{DF},\phi_{DF}]Y_2{}^{b'}[\beta_{DF},\phi_{DF}]\delta_{b-b',kN} \quad (10)$$

in which τ_m is the overall rotational correlation time constant for the molecule, $\mathbf{D}_{a,b}{}^{2}[\Omega_{MD}(t)]$ are Wigner rotation matrices,[36] the time-dependent Euler angles $\Omega_{MD}(t) = \{\alpha_{MD}(t),\beta_{MD}(t),\gamma_{MD}(t)\}$ describe the motions of the D frame relative to the M frame, $Y_2{}^{b}[\beta_{DF},\phi_{DF}]$ are modified spherical harmonic functions,[36] and $\{\beta_{DF},\phi_{DF}\}$ are the constant polar angles defining the orientation of $\mu(t)$ in the D reference frame. The Kronecker delta function, $\delta_{b-b',kN}$, with k and N integers, expresses the requirement that $G(\tau)$ be invariant under rotation by $2\pi/N$ if the molecular group that contains $\mu(t)$ has N-fold rotational symmetry about the z-axis of the D frame. Evaluation of eq 10 for a time satisfying the inequalities $\tau_e \ll \tau \ll \tau_m$, in which τ_e is the characteristic time for internal motions, yields a definition of the square of the generalized order parameter:[34]

$$S^2 = \sum_{a=-2}^{2}\sum_{b=-2}^{2}\sum_{b'=-2}^{2} \langle D_{a,b}{}^{2*}[\Omega_{MD}(t)]\rangle\langle \mathbf{D}_{a,b'}{}^{2}[\Omega_{MD}(t)]\rangle \times Y_2{}^{b*}[\beta_{DF},\phi_{DF}]Y_2{}^{b'}[\beta_{DF},\phi_{DF}]\delta_{b-b',kN} \quad (11)$$

For convenience, S^2 will be referred to simply as the order parameter. The order parameter satisfies the inequalities $0 \le S^2 \le 1$ with $S^2 = 0$ if the internal motions are isotropic and $S^2 = 1$ if the internal motions are completely restricted. Order parameters commonly are interpreted as a measure of the conformational restriction of $\mu(t)$; however, values of $S^2 = 0$ also can be obtained for particular models of restricted internal motions. For example, one simple specific physical model depicts the motions of a unit vector as free diffusion within a cone of semiangle β_0.[38,39] The order parameter is calculated from eq 11 using $\beta_{DF} = 0$ and $\phi_{DF} = 0$ to be

$$S^2 = [{}^1/_2 \cos\beta_0(1 + \cos\beta_0)]^2 \quad (12)$$

and $S^2 = 0$ for $\beta_0 = \pi/2$, as well as for $\beta_0 = \pi$.

Equations 10 and 11 implicitly define the conditions under which two different vectors with fixed relative orientations have identical autocorrelation functions or order parameters. If the orientation in the D frame of the first vector, $\mu(t)$, is defined by $\{\beta_{DF},\phi_{DF}\}$, then the orientation of a second vector $\mu'(t)$ can be expressed as $\{\beta_{DF}+\Delta\delta,\phi_{DF}+\Delta\phi\}$, in which $\Delta\beta = \beta'_{DF} - \beta_{DF}$ and $\Delta\phi = \phi'_{DF} - \phi_{DF}$ define the relative orientations of the two vectors. By substitution into eq 11, the correlation function for $\mu'(t)$ is

$$G'(\tau) = \exp[-\tau/\tau_m] \sum_{a=-2}^{2}\sum_{b=-2}^{2}\sum_{b'=-2}^{2} \langle \mathbf{D}_{a,b}{}^{2*}[\Omega_{MD}(0)]\mathbf{D}_{a,b'}{}^{2}[\Omega_{MD}(\tau)]\rangle \times Y_2{}^{b*}[\beta_{DF}+\Delta\beta,\phi_{DF}]Y_2{}^{b'}[\beta_{DF}+\Delta\beta,\phi_{DF}] \times \exp[i(b-b')\Delta\phi]\delta_{b-b',kN} \quad (13)$$

If $\mu(t)$ and $\mu'(t)$ are related by the N-fold rotational symmetry operation, then the two vectors have identical autocorrelation functions under all circumstances because $\Delta\beta = 0$ and $\Delta\phi = 2\pi m/N$ with m equal to an integer. If $\mu(t)$ and $\mu'(t)$ are not related by rotational symmetry, then the autocorrelation functions for the two vectors are identical if $\langle \mathbf{D}_{a,b}{}^{2*}[\Omega_{MD}(0)]\mathbf{D}_{a,b'}{}^{2}[\Omega_{MD}(\tau)]\rangle = \delta_{b,b'}\langle \mathbf{D}_{a,b}{}^{2*}[\Omega_{MD}(0)]\mathbf{D}_{a,b}{}^{2}[\Omega_{MD}(\tau)]\rangle$ and either $\Delta\beta = 0$ or $\Delta\beta = \pi - 2\beta_{DF}$. The first condition requires that the conditional probability distribution, $P[\Omega_{MD}(\tau)|\Omega_{MD}(0);\tau]$, which describes the time-dependent change in orientation of the D frame from $\Omega_{MD}(0)$ to $\Omega_{MD}(\tau)$, have at least five-fold rotational symmetry with respect to $\gamma_{MD}(t)$; that is, $P[\Omega_{MD}(\tau)|\Omega_{MD}(0);\tau] = P[\Omega_{MD}(\tau,k)|\Omega_{MD}(0,k);\tau]$, in which $\Omega_{MD}(t,k) = \{\alpha_{MD}(t),\beta_{MD}(t),\gamma_{MD}(t)+2\pi k/N\}$, $k = 0$ to $N-1$, and $N \ge 5$. If the conditional probability distribution has N-fold symmetry, then the equilibrium probability distribution, $P[\Omega_{MD}(t)]$, also has N-fold symmetry. The Euler angles $\alpha_{MD}(t)$, $\beta_{MD}(t)$, and $\gamma_{MD}(t)$ describe the motions relative to the M frame of a director that is collinear with the z-axis of the D frame coupled with rotational motion of $\mu(t)$ about the director axis. If motion of the director axis and rotational motion of the bectors about the director axis are independent, then one of the two types of motions must have at least five-fold symmetry. Thus, for example, autocorrelation functions for C^{β}–$H^{\beta 1}$ and C^{β}–$H^{\beta 2}$ bond vectors are identical if the conditional probability for motion of the C^{α}–C^{β} bond or for changes in the χ_1 angle has at least five-fold symmetry (assuming independence of the two motions).

If the equilibrium probability distribution, $P[\Omega_{MD}(t)]$, is at least three-fold symmetric with respect to $\gamma_{MD}(t)$, then the order parameters for $\mu(t)$ and $\mu'(t)$ are related to each other by

$$S'^2 = d_{00}{}^2(\beta_{DF} + \Delta\beta)^2 \sum_{a=-2}^{2} \langle \mathbf{D}_{a,0}{}^{2}[\Omega_{MD}(t)]\rangle^2 = d_{00}{}^2(\beta_{DF} + \Delta\beta)^2 S_z{}^2 = S^2[d_{00}{}^2(\beta_{DF} + \Delta\beta)/d_{00}{}^2(\beta_{DF})]^2 \quad (14)$$

in which $S_z{}^2$ is the order parameter for a unit vector aligned along the z-axis of the D frame and $d_{00}{}^2$ is a reduced Wigner matrix element.[36] Again, the order parameters are equal if either $\Delta\beta = 0$ or $\Delta\beta = \pi - 2\beta_{DF}$. Thus, the order parameters may be identical even if the autocorrelation functions differ. The orientation of the z-axis of the D frame is not required to be parallel to any covalent bonds in the molecule; observation of different order parameters for vectors with fixed relative orientations implies that no axis exists with $\beta'_{DF} = \beta_{DF}$ or $\beta_{DF} = \pi - \beta_{DF}$, about which the probability distribution of $\gamma_{MD}(t)$ is at least three-fold symmetric.

The ensemble average in eq 11 can be calculated using a specific physical model for the molecular motions or approximated by a simpler function without reference to a specific motional model. The two theoretical approaches are not exclusive; the parameters of a model-free formalism can be expressed in terms of the parameters of a specific motional model. In either instance, the parameters of the autocorrelation functions are determined by analysis of the experimental data. The model-free formalism of Lipari and Szabo[34] approximates $G(\tau)$ as

$$G(\tau) = \exp[-\tau/\tau_m]\{S^2 + (1 - S^2)\exp[-\tau/\tau_e]\} \quad (15)$$

in which τ_e is the effective correlation time. Using eqs 6 and 7, the auto-spectral density function is

$$J(\omega) = {}^2/_5[S^2\tau_m/(1 + \omega^2\tau_m{}^2) + (1 - S^2)\tau/(1 + \omega^2\tau^2)] \quad (16)$$

with $\tau = (1/\tau_m + 1/\tau_e)^{-1}$. Equations 15 and 16 contain a minimum set of adjustable parameters that characterize internal motions and have proven to be extremely useful in the analysis of NMR relaxation and fluorescence depolarization data. In the present study, internal motions with $\tau_e < 75$ ps are in the fast motional regime defined by Lipari and Szabo,[34] and eq 16 accurately represents the influence of these internal motions on ^{13}C spin relaxation.

(38) Kinosita, K.; Kawato, S.; Ikegami, A. *Biophys. J.* **1977**, *20*, 289–305.
(39) Lipari, G.; Szabo, A.; Levy, R. M. *Nature* **1982**, *300*, 197–198.

The autocorrelation function for a terminal methyl group of an amino acid side chain contains contributions from overall rotation, internal motion of the symmetry axis for the methyl group, and rotational motion of the methyl C–H bond vectors about the symmetry axis. The symmetry axis is defined by the carbon–carbon bond connecting the methyl group to the molecule (e.g. the C^{α}–C^{β} bond for Ala). In the present work, motion of the symmetry axis is described by diffusion within a cone of semiangle β_0 and the autocorrelation function for the symmetry axis is approximated by a single exponential function that has the correct value at long times and is exact to linear order in time.[40] In the first two models considered, methyl rotation is described by restricted rotational diffusion about the symmetry axis or by jump-like transitions between rotameric positions. The resulting autocorrelation function is[40]

$$G(\tau) = \exp[-\tau/\tau_m] \sum_{b=-2}^{2} \{S_0^2 + (1 - S_0^2) \exp[-\kappa_b \tau/\tau_0]\} \times \exp[-(1 - \beta_{b,0}) a^2 \tau/\tau_c][d_{b,0}^2(\beta_{DF})]^2 \quad (17)$$

in which $d_{b,0}$ is a reduced Wigner matrix element,[36] $\delta_{b,0}$ is the Kronecker delta function, S_0^2 is the order parameter for the methyl symmetry axis and is given in terms of β_0 by eq 12, $\kappa_b = (1 - b^2/6)$, τ_0 is the effective correlation time for motions of the methyl symmetry axis, $a = b$ for the diffusion model and $a = 1$ for the three-site jump model, τ_c is the characteristic time for methyl rotation, and β_{DF} is the angle between the symmetry axis and the C–H bond vectors. For the diffusion model, $\tau_c = 1/D$, in which D is the rotational diffusion constant for the methyl group; for the jump model, $\tau_c = 3/\lambda$, in which λ is the jump rate between rotamer positions. Using eqs 6, 7, and 17, the auto-spectral density function is

$$J(\omega) = {}^2/_5[\{S_0^2\tau_m/(1+\omega^2\tau_m^2) + (1-S_0^2)\tau_1/(1+\omega^2\tau_1^2)\}[d_{00}^2(\beta_{DF})]^2 + 2\{S_0^2\tau_2/(1+\omega^2\tau_2^2) + (1-S_0^2)\tau_3/(1+\omega^2\tau_3^2)\}[d_{10}^2(\beta_{DF})]^2 + 2\{S_0^2\tau_4/(1+\omega^2\tau_4^2) + (1-S_0^2)\tau_5/(1+\omega^2\tau_5^2)\}[d_{20}^2(\beta_{DF})]^2] \quad (18)$$

in which $\tau_1 = (1/\tau_m + 1/\tau_0)^{-1}$, $\tau_2 = (1/\tau_m + 1/\tau_c)^{-1}$, $\tau_3 = (1/\tau_m + {}^5/_6\tau_0 + 1/\tau_c)^{-1}$, $\tau_4 = (1/\tau_m + a^2/\tau_c)^{-1}$, and $\tau_5 = (1/\tau_m + {}^1/_3\tau_0 + a^2/\tau_c)^{-1}$. Comparison of eqs 11, 15, and 17 yields a relationship between the order parameter for a unit vector oriented along a C–H bond in a methyl group and the order parameter for the symmetry axis of the methyl group:

$$S^2 = S_0^2[d_{00}^2(\beta_{DF})]^2 = 0.1107 S_0^2 \quad (19)$$

in which $\beta_{DF} = 70.5°$ for ideal tetrahedral geometry.[41]

Experimental Methods

NMR Spectroscopy. Experiments were performed on a 10 mM solution of the zinc-complexed Xfin-31 peptide (Ac-YKCGLCERSFVEK-SALSRHQRVHKN-NH_2, ^{13}C at natural abundance) in D_2O at 303 K. NMR spectroscopy was performed using Bruker AM and AMX spectrometers at 11.7 and 7.0 T, which correspond to ^{13}C Larmor frequencies of 125.7 and 75.5 MHz, respectively. Proton-detected two-dimensional inversion–recovery, CPMG, and steady-state {^1H}–^{13}C NOE measurements used the pulse sequences of Figure 1. For inversion–recovery and CPMG experiments, a delay of 3 times the spin–lattice relaxation time for the ^{12}C isotopomer protons was used between acquisitions; for NOE experiments a delay of 7–10 times the ^{13}C spin–lattice relaxation time was used between acquisitions. The WALTZ-16 phase-modulation scheme[42] was used to saturate protons during the delay t of inversion–recovery experiments; the GARP-1 phase-modulation scheme[43] was used to saturate protons during the recovery delay of the NOE experiments. Proton decoupling using a train of 180° ^1H pulses was used during the delay t of the CPMG experiments for aromatic ^{13}C spins. A spin–echo period $\tau = 0.5$ ms was used for CPMG experiments. The WALTZ-16 phase-modulation scheme was used for decoupling ^{13}C during acquisition. Frequency discrimination in the ω_1 dimension was achieved using time-proportional phase incrementation.[44]

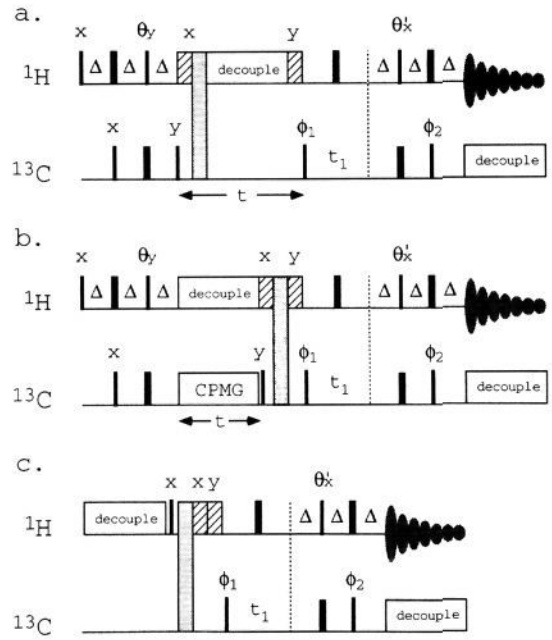

Figure 1. Pulse sequences for proton-detected heteronuclear relaxation measurements using two-dimensional proton-detected (a) inversion–recovery, (b) CPMG, and (c) steady-state NOE experiments. Thin and thick vertical bars represent 90° and 180° pulses, respectively, except for the pulses with rotation angles θ and θ'; hatched bars represent 1–2-ms high-power spin-lock purge pulses; and stippled bars represent 2–3-ms homogeneity-spoiling pulses followed by 7–8-ms delays to allow eddy currents to dissipate. Phases of the pulses are indicated in the figure, except for 180° pulses, which were applied with y phase. For AX spin systems, $\theta = \theta' = 90°$; for AX_3 spin systems, $\theta = 54.7°$ and $\theta' = 54.7°$ or 30°, as described in the text. For polarization transfer, $\Delta = 1/(2J_{XH})$. For inversion–recovery and CPMG experiments, t is the relaxation period, which is parametrically varied between two-dimensional spectra. For NOE experiments, spectra are acquired with (shown) and without (not shown) saturation of protons during the recovery period between acquisitions. In part a, proton saturation during t is achieved using a broad-band decoupling sequence or a train of closely spaced 180° pulses. In part b, a CPMG sequence that consists of an even number of repetitions of the spin–echo sequence τ–$180_x°$–τ is applied to the ^{13}C spins during t; proton decoupling is achieved by applying 180° pulses synchronously with the even echoes of the CPMG sequence. As discussed in the text, $\tau \approx 0.5$ is sufficient to minimize effects of evolution of antiphase terms in the density operator. The train of proton pulses during t can be omitted if cross-correlation between dipolar and CSA relaxation mechanisms is negligible. The basic phase cycling is $\phi_1 = (y\,{-y}\,y\,{-y})$, $\phi_2 = (x\,x\,{-x}\,{-x})$, and receiver $(x\,{-x}\,{-x}\,x)$; quadrature detection in the ω_1 dimension is achieved using time-proportional phase incrementation[44] or the hypercomplex method.[72,73] Weak presaturation of the solvent resonance was used in sequences a and b.

Aromatic ^{13}C Relaxation at 11.7 T. Spin–lattice relaxation rate constants, spin–spin relaxation rate constants, and steady-state NOE enhancements were measured at 11.7 T for the protonated aromatic ^{13}C spins of Tyr 1, Phe 10, His 19, and His 23 in Xfin-31. For inversion–recovery experiments, 11 spectra were acquired using delays t of 12, 52, 92, 130, 210, 290, 410, 530, 810, 1010, and 1490 ms. Eleven spectra were acquired for the CPMG experiment using delays t of 9 (two spectra), 21, 39, 66, 99, 200, 300, 500, 800, and 1200 ms. For each spectrum, 64 free-induction decays were averaged per t_1 increment. For NOE

(40) Brainard, J. R.; Szabo, A. *Biochemistry* **1981**, *20*, 4618–4628.
(41) Lipari, G.; Szabo, A. *J. Am. Chem. Soc.* **1982**, *104*, 4559–4570.
(42) Shaka, A. J.; Keeler, J.; Frenkiel, T.; Freeman, R. *J. Magn. Reson.* **1983**, *52*, 335–338.
(43) Shaka, A. J.; Barker, P. B.; Freeman, R. *J. Magn. Reson.* **1985**, *64*, 547–552.
(44) Marion, D.; Wüthrich, K. *Biochem. Biophys. Res. Commun.* **1983**, *113*, 967–974.

experiments, two spectra were acquired with proton saturation and three were acquired without saturation. For each spectrum, 128 FIDs were averaged per t_1 increment. In all instances, 50–64 experiments were recorded in t_1; the spectral widths were 3205 and 5000 Hz in ω_1 and ω_2, respectively. The radiofrequency transmitters were set to 127 ppm for ^{13}C and 4.7 ppm for ^1H.

Methyl ^{13}C Relaxation. Spectra were obtained for the terminal methyl groups of Leu 5, Val 11, Ala 15, Leu 16, and Val 22. The assignments of the resonances have been reported previously.[45] Stereospecific assignments of geminal methyl groups are available only for Leu 16 (Lee, M. S.; Wright, P. E. Unpublished results); for the other residues, the more upfield of the two geminal ^{13}C resonances arbitrarily has been designated spin "a" and the more downfield resonance has been designated spin "b" (see Results). A pulse flip angle of $\theta = 54.7°$ (Figure 1) was used to minimize systematic errors due to relaxation of multiple spin components of the density operator and a pulse flip angle of $\theta' = 30°$ was used to maximize sensitivity.[46] For comparison, an additional inversion–recovery experiment was performed at 11.7 T with $\theta = \theta' = 54.7°$. At 7.0 T, spin–lattice relaxation rate constants and steady-state NOE enhancements were measured for the methyl ^{13}C spins in Xfin-31. For inversion–recovery experiments, 10 spectra were acquired using delays t of 39 (two spectra), 58, 97, 150, 210, 310, 400, 500, 670, 860, and 1250 ms. For each spectrum, 256 free-induction decays were averaged per t_1 increment. For NOE experiments, three spectra were acquired with proton saturation and three were acquired without saturation. For each spectrum, 512 FIDs were averaged per t_1 increment. In all cases, 100 experiments were recorded in t_1; the spectral widths were 1000 and 4000 Hz in ω_1 and ω_2, respectively. The radiofrequency transmitters were set to 20 ppm for ^{13}C and 2.4 ppm for ^1H. At 11.7 T, spin–lattice relaxation rate constants, spin–spin relaxation rate constants, and steady-state NOE enhancements were measured for the methyl ^{13}C spins in Xfin-31. For inversion–recovery experiments, ten spectra were acquired using delays t of 34 (two spectra), 91, 210, 300, 490, 860, 1240, 1740, and 2490 ms. Ten spectra were acquired for the CPMG experiment using delays t of 8 (two spectra), 36, 76, 150, 300, 500, 750, 1250, and 2000 ms. For each spectrum, 64 free-induction decays were averaged per t_1 increment. Relaxation rate constants were measured in two independent experiments and averaged. For NOE experiments, three spectra were acquired with proton saturation and three were acquired without saturation. For each spectrum, 128 FIDs were averaged per t_1 increment. In all instances, 50 experiments were recorded in t_1; the spectral widths were 1634 and 5000 Hz in ω_1 and ω_2, respectively. The radiofrequency transmitter frequencies were 22 ppm for ^{13}C and 1.4 ppm for ^1H.

NMR Data Processing. Spectra were Fourier transformed using a matched exponential filter in t_2 and a Kaiser apodization function in t_1. The first point in each dimension was halved prior to Fourier transformation.[47] The data was zero filled once in t_2 and twice in t_1. Phenomenological spin–lattice, R_1, and spin–spin, R_2, relaxation rate constants were determined by nonlinear fits of the equations

$$I(t) = I_\infty - [I_\infty - I_0] \exp(-R_1 t) \tag{20}$$

$$I(t) = I_0 \exp(-R_2 t) + I_\infty \tag{21}$$

in which $I(t)$ are the peak heights in the spectra acquired with a parametric relaxation period, t; I_0 are the initial values of the peak heights; and I_∞ are the steady-state values of the peak heights as $t \rightarrow \infty$. The fitting routine used a Levenburg–Marquardt algorithm.[48] Magnetization may decay to a nonzero steady-state value in CPMG experiments due to pulse imperfections;[49] consequently, spin–spin relaxation data were fit with two free parameters ($I_\infty = 0$) or with three free parameters ($I_\infty \neq 0$). An F-test was used to test whether I_∞ differed significantly from zero in the three-parameter fit.[19] The NOE enhancements were calculated from

$$\eta = \langle I_{sat} \rangle / \langle I_{unsat} \rangle - 1 \tag{22}$$

in which $\langle I_{sat} \rangle$ and $\langle I_{unsat} \rangle$ are the average peak heights in spectra acquired with and without proton saturation during the recovery delay. Uncertainties in peak heights and relaxation parameters were determined as described previously.

If the effects of cross-correlation between C–H vectors are substantial, the relaxation of methyl ^{13}C spins is biexponential,[32,50] and the phenomenological rate constants extracted from the relaxation data by a single-exponential fit using eqs 20 and 21 are biased. To assess the magnitude of the potential errors in the present case, the spin–lattice relaxation rate matrix for an isolated AX_3 spin system was calculated using expressions for matrix elements given elsewhere.[32,50] Auto-spectral densities were calculated using eq 18; cross-spectral densities, $K(\omega)$, were calculated using a generalization of eq 18 to include cross-correlation between pairs of C–H or H–H bond vectors:

$$K(\omega) = {}^2/_5[\{S_0^2\tau_m/(1+\omega^2\tau_m^2) + (1-S_0^2)\tau_1/(1+\omega^2\tau_1^2)\}[d_{00}^2(\beta_{DF})]^2 + 2\{S_0^2\tau_2/(1+\omega^2\tau_2^2) + (1-S_0^2)\tau_3/(1+\omega^2\tau_3^2)\}[d_{10}^2(\beta_{DF})]^2 \cos\xi + 2\{S_0^2\tau_2/(1+\omega^2\tau_2^2) + (1-S_0^2)\tau_3/(1+\omega^2\tau_4^2)\}[d_{20}^2(\beta_{DF})]^2 \cos(2\xi)] \tag{23}$$

in which ξ is the azimuthal angle between the two vectors. For cross-correlation between C–H vectors, $\beta = 70.5°$ and $\xi = 120°$; for H–H vectors, $\beta = 90°$ and $\xi = 60°$. Calculations were performed with a range of parameters consistent with the results of Tables VI and VII. Biexponential decay curves were calculated from the rate matrix using the same time points employed in the experimental measurements and were fit with eq 20 to obtain apparent monoexponential rate constants. Theoretical values of η were calculated from the spin–lattice relaxation rate matrix.[32]

Analysis of NMR Relaxation Parameters. The ^{13}C NMR relaxation parameters were analyzed using eqs 1–5 and the model-free auto-spectral density function (eq 16). The overall rotational correlation time, order parameters, and effective internal correlation times were calculated by a nonlinear least squares optimization, as described previously[10] by minimizing the approximate χ^2 variable given by

$$\chi^2 = \sum_{i=1}^{M} \chi_i^2 = \sum_{i=1}^{M} \sum_{j=1}^{N} (R_{ij} - \hat{R}_{ij})^2 / \sigma_{ij}^2 \tag{24}$$

in which M is the number of carbon spins included in the analysis, N is the total number of measured relaxation parameters (R_1, R_2, and NOE) available for each spin, R_{ij} is the experimental value of the jth relaxation parameter for the ith carbon spin, $\hat{R}_{ij}$ is the corresponding value calculated from the model-free parameters, and σ_{ij} is the corresponding uncertainty in the experimental parameter. Equation 24 standardizes the differences between the measured and predicted relaxation parameters using the uncertainties in the experimental parameters; accordingly, the most precise measurements are most influential in determining the parameters of the auto-spectral density function. Herein, eq 24 will be called the absolute minimization function. The analysis was also performed by minimizing the alternative χ^2 variable used in other studies,[9,13,14]

$$\chi^2 = \sum_{i=1}^{M} \chi_i^2 = \sum_{i=1}^{M} \sum_{j=1}^{3} (R_{ij} - \hat{R}_{ij})^2 / R_{ij}^2 \tag{25}$$

which depends upon the fractional differences between the measured and predicted relaxation parameters. Herein, eq 25 will be called the relative minimization function. Uncertainties in the fitted model-free parameters were estimated by Monte Carlo simulations. The values of the constants in eqs 4 and 5 are the following: $\hbar = 1.054 \times 10^{-3}$ J s, $\mu_0 = 4\pi \times 10^{-7}$ T m A^{-1}, $\gamma_H = 2.6752 \times 10^8$ s^{-1} T^{-1}, $\gamma_C = 6.728 \times 10^7$ s^{-1} T^{-1}, $r_{CH} = 1.07 \times 10^{-10}$ m, $\omega_H = 2\pi \times 300.13$ MHz at 7.0 T, $\omega_H = 2\pi \times 499.874$ MHz at 11.7 T, $\omega_C = 2\pi \times 75.5$ MHz at 7.0 T, and $\omega_C = 2\pi \times 125.7$ MHz at 11.7 T. Values of $\Delta\sigma$ used for the aromatic ^{13}C spins are given in Table I. The value of $\Delta\sigma$ for methyl carbons is sufficiently small ($\Delta\sigma = 25$ ppm) that CSA has a negligible effect on relaxation; according $\Delta\sigma$ was set to zero for methyl spins. R_a was included as an optimizable parameter in eq 2 for His 19, His 23, Leu 5, and Val 22, because analysis of the backbone C^α dynamics for these residues had suggested the presence of chemical-exchange contributions to R_2.[10] Analyses for methyl spins were performed using all the relaxation parameters acquired at 7.0 and 11.7 T and using only R_1 and η determined at the two magnetic fields. An additional analysis of the relaxation parameters for the methyl spins was performed using the auto-spectral density function for the diffusion

(45) Lee, M. S.; Palmer, A. G.; Wright, P. E. *J. Biomol. NMR* **1992**, *2*, 307–322.

(46) Palmer, A. G.; Wright, P. E.; Rance, M. *Chem. Phys. Lett.* **1991**, *185*, 41–46.

(47) Otting, G.; Widmer, H.; Wagner, G.; Wüthrich, K. *J. Magn. Reson.* **1986**, *66*, 187–193.

(48) Press, W. H.; Flannery, B. P.; Teukolsky, S. A.; Vetterling, W. T. *Numerical Recipes. The Art of Scientific Computing*; Cambridge University Press: Cambridge, U.K. 1986.

(49) Vold, R. L.; Vold, R. R.; Simon, H. E. *J. Magn. Reson.* **1973**, *11*, 283–298.

(50) Kay, L. E.; Torchia, D. A. *J. Magn. Reson.* **1991**, *95*, 536–547.

Table I. Chemical Shift Anisotropy Values for Aromatic Amino Acids[a]

residue	σ_{11} (ppm)	σ_{22} (ppm)	σ_{33} (ppm)	σ_{iso} (ppm)	$\Delta\sigma$ (ppm)
Tyr	225	149	15	130	−172
Phe	225	149	15	130	−172
His	217	124	48	130	−123

[a] Values of σ_{11}, σ_{22}, and σ_{33} for Tyr and Phe are quoted as the average values determined experimentally for a series of substituted benzene derivatives.[65] Values of σ_{11}, σ_{22}, and σ_{33} for His are the average of theoretical results for the δ and ϵ nuclei.[64] The isotropic shift is given by $\sigma_{iso} = (\sigma_{11} + \sigma_{22} + \sigma_{33})/3$; $\Delta\sigma = \sigma_{11} - (\sigma_{22} + \sigma_{33})/2$. The values quoted for Phe and Tyr are referenced relative to TMS. For comparison to the results for Phe and Tyr, the quoted values for His have been scaled arbitrarily to give an isotropic shift of 130 ppm; the value of $\Delta\sigma$ is unaffected by this change. The values of $\Delta\sigma$ presented are similar to those measured experimentally for the C^{γ} nuclei of His.[63]

model for methyl rotation (eq 18; $a = b$); values of S_0^2, τ_0 and τ_e were optimized for each methyl spin by minimizing eq 24.

Time-Resolved Fluorescence Spectroscopy. Experiments were performed on a 70 μM solution of the zinc-complexed peptide in H_2 at 283, 293, and 303 K and a 100 μM solution of the zinc-free peptide in H_2O at 303 K. The latter solution also contained 2 mM dithiothreitol to prevent oxidation of free sulfhydryl groups in the peptide. Time-resolved fluorescence measurements were obtained for Tyr 1 in Xfin-31 using the laser fluorescence decay spectrometer described previously.[51] Briefly, samples were contained in a quartz cuvette inside a temperature-controlled housing; fluorescence was excited using the frequency-doubled output of a synchronously mode-locked and cavity-dumped dye laser pumped by a mode-locked argon ion laser; fluorescence emission perpendicular to the excitation beam was collimated, passed through a polarizer, dispersed by a monochromator, and detected using a microchannel plate photomultiplier. Fluorescence was excited at 286 nm and observed at 300 nm using a band-pass of 4 nm. Time-resolved fluorescence emission decay curves were measured by time-correlated single-photon counting. The decays of intensity polarized parallel and perpendicular to the vertical polarization of the excitation pulse were measured by rotating the polarizer located between the sample and the monochromator. Emission curves were measured using sampling intervals of 9.55 and 35.91 ps/channel. The instrument response function was measured from light scattered by a suspension of nondairy coffee creamer. The full width at half height of the response function was typically 45 ps. The fluorescence decay curves were analyzed using the following expressions:

$$I_{\parallel}(t) = R(t) \otimes \{[1 + 2r(t)]K(t)\} \quad (26)$$

$$I_{\perp}(t) = gR(t) \otimes \{[1 + r(t)]K(t)\} \quad (27)$$

in which $R(t)$ is the instrument response function, g is a factor expressing the small polarization bias of the detection system, $K(t)$ describes the ideal decay of the total fluorescence intensity, $r(t)$ is the time-dependent fluorescence polarization anisotropy, and $\otimes$ is the convolution operator. Both $K(t)$ and $r(t)$ are assumed to be expressible as sums of exponential functions:

$$K(t) = \sum_{i=1}^{N} \alpha_i \exp[-t/\tau_i] \quad (28)$$

$$r(t) = \sum_{j=1}^{M} r_{0j} \exp[-t/\tau_{rj}] \quad (29)$$

in which τ_i and τ_{rj} are the fluorescence lifetimes and anisotropy decay times, respectively, α_i is the fractional amplitude associated with the ith lifetime, and r_{0j} is the limiting anisotropy associated with the jth anisotropy decay time. If τ_{r1} is taken to be the overall rotational correlation time of the molecule, τ_m, then

$$r(t) = \exp[-t/\tau_m]\{r_{01} + \sum_{j=2}^{M} r_{0j} \exp[-t/\tau_{rj}]\} \quad (30)$$

in which

$$\hat{\tau}_{rj} = (1/\tau_{rj} - 1/\tau_m)^{-1} \quad (31)$$

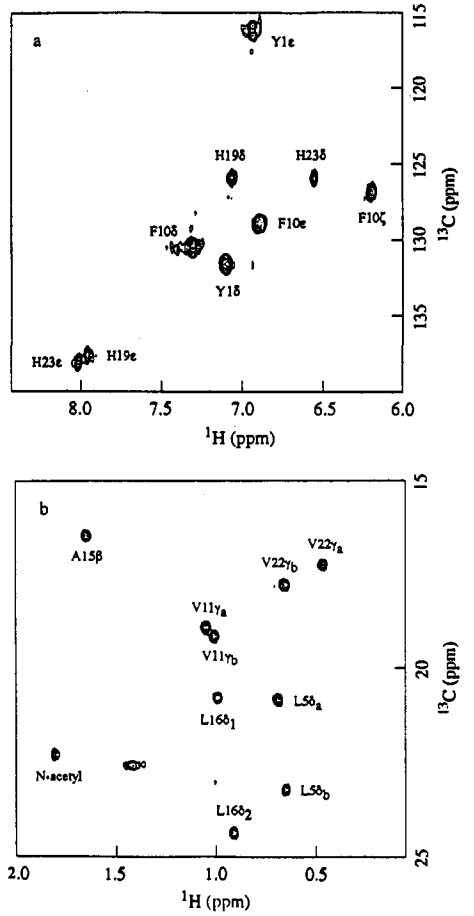

Figure 2. Typical ^{13}C–^1H correlation NMR spectra for (a) aromatic and (b) methyl groups in Xfin-31. Spectra shown were acquired with the inversion–recovery pulse sequence (Figure 1a) and a minimum relaxation delay t. The sequence-specific assignments indicated have been reported elsewhere.[45] Stereospecific assignments of the geminal methyl resonances have been obtained only for Leu 16; for other Val and Leu residues, the upfield ^{13}C resonance of the two methyl spins has been labeled methyl "a" and the downfield resonance has been labeled methyl "b".

The order parameter and effective internal correlation time are defined as, respectively

$$S^2 = r_{01} / \sum_{j=1}^{M} r_{0j} \quad (32)$$

$$\tau_e = \sum_{j=2}^{M} r_{0j} \hat{\tau}_{rj} / \sum_{j=2}^{M} r_{0j} \quad (33)$$

Experimental fluorescence depolarization data for $I_{\parallel}(t)$ and $I_{\perp}(t)$ were simultaneously fit by eqs 26–29 with $\{\alpha_i\}$, $\{\tau_i\}$, $\{r_{0j}\}$, and $\{\tau_{rj}\}$ as optimizable parameters. The values of M and N were parametrically varied between analyses, and the quality of the resulting fits were judged from the values of the reduced χ^2 values and from graphs of the weighted residuals. The factor $g = 1.002$ was determined from $I_{\parallel}(t)$ and $I_{\perp}(t)$ acquired at 35.91 ps/channel by matching the latter portions of the curves after the polarization anisotropy had decayed to zero. The same g factor was used for curves acquired using 9.55 ps/channel. Curve fitting used the Levenburg–Marquardt algorithm;[48] the convolution integral was evaluated numerically using recursion relations.[52]

Results

Contour plots of the two-dimensional spectra obtained for the initial delay in the inversion–recovery experiments at 11.7 T are shown in Figure 2a and b for the aromatic and methyl resonances, respectively. All resonances were resolved sufficiently to permit accurate determinations of peak heights in the spectra. The signal-to-noise ratios for peaks in the spectra shown are 20–30; similar

(51) Guest, C. R.; Hochstrasser, R. A.; Sowers, L. C.; Millar, D. P. *Biochemistry* **1991**, *30*, 3271–3279.

(52) Grinvald, A.; Steinberg, I. Z. *Anal. Biochem.* **1974**, *59*, 583–598.

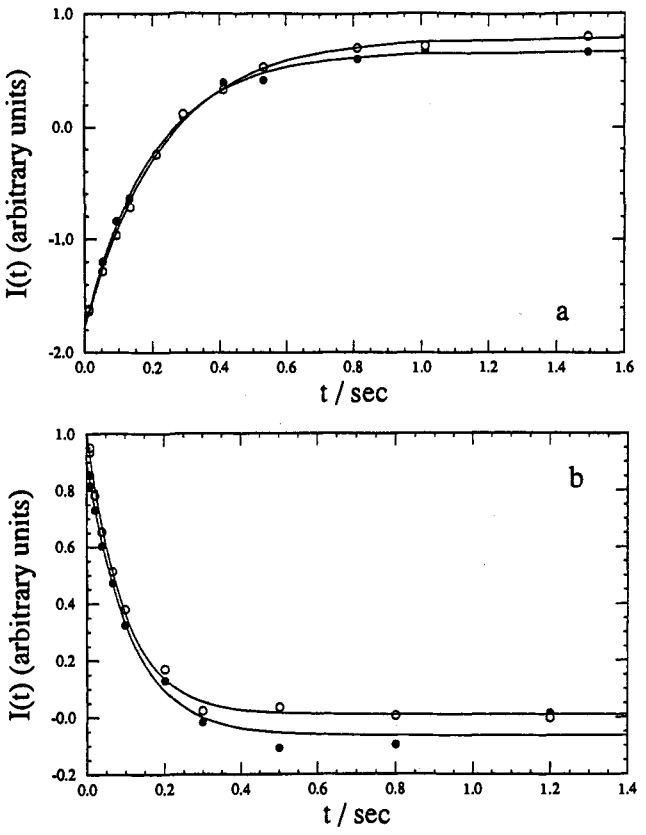

Figure 3. Experimental spin-relaxation curves for the protonated aromatic ^{13}C spins of Tyr 1. Shown are (a) the inversion–recovery curves for measuring spin–lattice relaxation and (b) the CPMG curves for measuring spin–spin relaxation of the δ (●) and ϵ (○) ^{13}C spins. Solid lines are the best nonlinear least squares fits to (a) eq 20 and (b) eq 21. The CPMG data for the δ spin was fit statistically better by eq 21 when a baseline offset, $I_\infty \neq 0$, was included as a free parameter. Residual χ^2 values obtained from the nonlinear curve fits indicated that the model functions eqs 20 and 21 adequately described the relaxation data. Uncertainties in the peak intensities (not shown) are equal to the root-mean-square baseline noise in the spectra and are approximately 1–2 times the size of the plotted symbols.

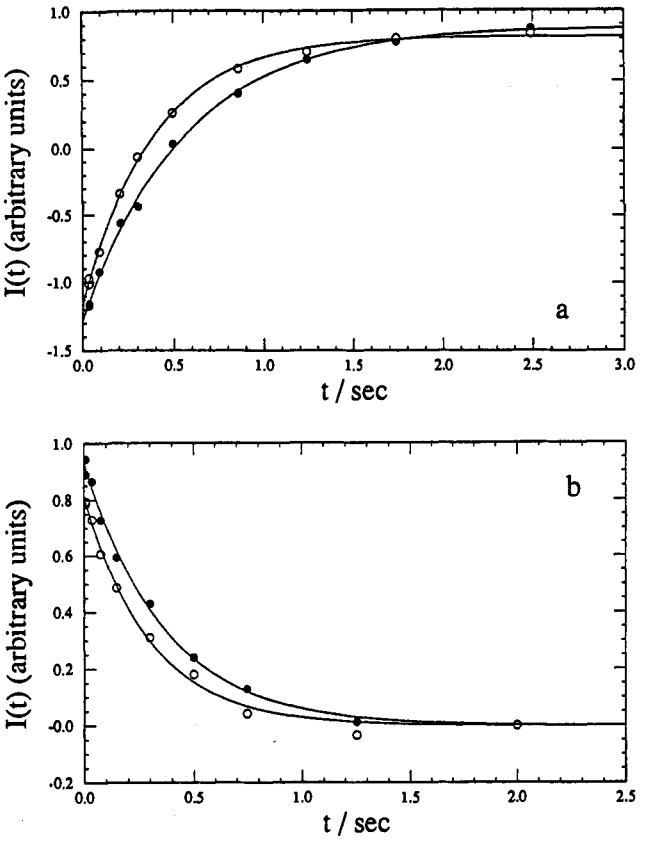

Figure 4. Experimental spin-relaxation curves for the $^{13}C^{\gamma}$ spins of Val 11. Shown are (a) the inversion–recovery curves for measuring spin–lattice relaxation and (b) the CPMG curves for measuring spin–spin relaxation of the γ_a (●) and γ_b (○) ^{13}C spins. Solid lines are the best nonlinear least squares fits to (a) eq 20 and (b) eq 21. Residual χ^2 values obtained from the nonlinear curve fits indicated that the model functions eqs 20 and 21 adequately described the relaxation data. Uncertainties in the peak intensities (not shown) are equal to the root-mean-square baseline noise in the spectra and are approximately the size of the plotted symbols.

sensitivities were obtained in CPMG and NOE experiments. Single resonances are observed for the δ and ϵ spins of Tyr 1 and Phe 10; thus the rate of chemical exchange of the δ_1 and δ_2 spins and of the ϵ_1 and ϵ_2 spins due to ring flipping is large compared with the chemical shift differences between the symmetry-related spins.[35] As is evident in Figure 2a, the peak shapes for Tyr 1 C^{ϵ} and Phe 10 C^{δ} are slightly distorted; for these two resonances, chemical shift differences between the symmetry-related spins may be large enough that the dynamics of the ring-flip process approach the intermediate exchange regime.

Typical spin–lattice and spin–spin decay curves are shown in Figure 3a and b, respectively, for the δ and ϵ ^{13}C spins of Tyr 1 and in Figure 4a and b for the γ_1 and γ_2 ^{13}C spins of Val 11. Relaxation rate constants obtained from the experimental data by nonlinear least squares fitting of eqs 20 and 21 and steady-state NOE enhancements calculated from eq 22 are given in Table II for aromatic carbon spins and in Table III for methyl carbon spins. Inversion–recovery curves were well fit statistically using eq 20 with three free parameters. The CPMG curves generally were well fit using eq 21 with two free parameters and $I_\infty = 0$; for a small number of aromatic residues, including the C^{δ} of Tyr 1 (Figure 3b), the decay curves were fit better statistically by eq 21 with three free parameters ($I_\infty \neq 0$). Uncertainties in the optimized values of R_1 and R_2 generally are 2–10%. Uncertainties in η generally are 5–25% for aromatic ^{13}C spins and 2–5% for methyl ^{13}C spins.

Table II. Relaxation Parameters for Aromatic ^{13}C Spins in Xfin-31[a]

nucleus	R_1 (s^{-1})	R_2 (s^{-1})	η
Tyr 1 δ	4.87 ± 0.16	10.6 ± 0.6	0.16 ± 0.01
Tyr 1 ϵ	4.32 ± 0.14	10.1 ± 0.6	0.20 ± 0.04
Phe 10 δ	4.96 ± 0.18	12.4 ± 0.7	0.21 ± 0.03
Phe 10 ϵ	5.57 ± 0.21	14.0 ± 1.0	0.11 ± 0.02
Phe 10 ζ	5.10 ± 0.44	16.4 ± 2.3	0.11 ± 0.06
His 19 δ	4.53 ± 0.20	11.1 ± 0.8	0.22 ± 0.03
His 19 ϵ	4.66 ± 0.26	16.5 ± 1.6	0.16 ± 0.04
His 23 δ	4.21 ± 0.26	16.5 ± 1.7	0.23 ± 0.04
His 23 ϵ	4.00 ± 0.25	11.9 ± 1.2	0.27 ± 0.07

[a] Relaxation parameters were determined from experimental NMR data using eqs 22–24. Uncertainties were determined as described in the text.

Previous work demonstrated that R_1 values for $NaCO_2CH_3$ measured by proton-detected techniques agreed with values measured by conventional direct-detect inversion–recovery experiments if flip angles of 54.7°, the magic angle, were used for the editing pulse in the polarization-transfer sequences.[46] Similar results have been obtained for fractionally ^{13}C enriched calbindin D_{9k}, a 75 amino acid protein with a rotational correlation time of 4 ns (Palmer, A. G. Unpublished results). In the present work, inversion–recovery experiments in which $\theta = 54.7°$ and $\theta' = 30°$ yielded the same results as experiments in which $\theta = \theta' = 54.7°$; however, the former sequences were approximately 40% more sensitive (data not shown). No statistical evidence was obtained for biexponential-decay curves for methyl ^{13}C spins in inversion–recovery experiments. The magnitudes of cross-

Table III. Relaxation Parameters for Methyl ^{13}C Spins in Xfin-31[a]

	7.0 T		11.7 T		
nucleus	R_1 (s^{-1})	η	R_1 (s^{-1})	R_2 (s^{-1})	η
Leu 5 δ_a	1.70 ± 0.15	0.88 ± 0.07	1.38 ± 0.04	2.30 ± 0.10	1.20 ± 0.03
Leu 5 δ_b	2.67 ± 0.18	1.13 ± 0.11	2.20 ± 0.06	4.51 ± 0.25	1.26 ± 0.03
Val 11 γ_a	2.62 ± 0.18	1.02 ± 0.09	1.83 ± 0.04	2.79 ± 0.11	1.15 ± 0.03
Val 11 γ_b	3.56 ± 0.23	1.06 ± 0.08	2.56 ± 0.06	3.45 ± 0.16	1.04 ± 0.03
Ala 15 β	6.61 ± 0.47	0.89 ± 0.09	4.56 ± 0.15	7.24 ± 0.52	1.12 ± 0.04
Leu 16 δ_1	4.03 ± 0.34	0.87 ± 0.11	3.35 ± 0.12	6.65 ± 0.51	1.05 ± 0.04
Leu 16 δ_2	3.08 ± 0.22	0.91 ± 0.06	2.32 ± 0.07	3.98 ± 0.22	0.99 ± 0.04
Val 22 γ_a	3.01 ± 0.30	0.71 ± 0.12	1.75 ± 0.07	4.40 ± 0.31	1.05 ± 0.04
Val 22 γ_b	3.17 ± 0.21	1.06 ± 0.11	2.62 ± 0.07	4.40 ± 0.23	1.13 ± 0.04

[a] Relaxation parameters were determined from experimental NMR data using eqs 22–24. Uncertainties were determined as described in the text.

Table IV. Model-Free Parameters for Aromatic ^{13}C Spins in Xfin-31[a]

nucleus	S^2	R_a (s^{-1})	χ_r^2
Tyr 1 δ	0.77 ± 0.03		11.1
Tyr 1 ϵ	0.71 ± 0.03		0.01
Phe 10 δ	0.79 ± 0.04		1.2
Phe 10 ϵ	0.95 ± 0.04		15.0
Phe 10 ζ	0.91 ± 0.04		4.1
His 19 δ	0.86 ± 0.04		0.42
His 19 ϵ	0.90 ± 0.04	5.5 ± 0.2	0.75
His 23 δ	0.78 ± 0.04	6.8 ± 0.1	0.0
His 23 ϵ	0.73 ± 0.03		0.05

[a] Shown are the order parameters and exchange contributions to the phenomenological R_2 calculated from the relaxation data of Table III using eqs 1–5 and 16. Parameters were determined by minimizing eq 24. As indicated by Monte Carlo simulations, the effective correlation times could not be determined reliably and are not reported. The overall rotational correlation time was determined to be 1.8 ± 0.1 ns (at 303 K in D_2O).

correlation effects also were assessed from spin–lattice relaxation rate matrices calculated using the spectral density functions given by eqs 18 and 23. The monoexponential rate constants obtained from fitting eq 20 to decay curves calculated from the spin–lattice relaxation rate matrices differ from the matrix elements for the single-quantum operators by <5%, which is comparable to the statistical uncertainties in the measured rate constants. In addition, errors in η of <10% are predicted from the calculated spin–lattice rate matrix. The above analysis assumes that the methyl group is isolated; in practice, dipolar interactions between the methyl protons and nearby protons in the protein further reduce the errors introduced by cross-correlation.[32,50] No statistical evidence was obtained for biexponential decay curves for methyl ^{13}C spins in CPMG experiments. Representative spin–spin relaxation rate matrices were not calculated theoretically; however, internal motional parameters calculated from the relaxation data are unchanged if the R_2 values are excluded from the analysis (see below). Consequently, the effects of cross-correlation on the R_2 values measured in the present study are expected to be small. A recent report indicates that, for proteins larger than Xfin-31, cross-correlation in methyl groups biases measurements of R_2 more strongly than measurements of R_1.[53]

Values of the parameters for the Lipari–Szabo model-free formalism for the aromatic ^{13}C spins are given in Table IV. Results were calculated from the data of Table II using eqs 1–5 and 16 and the absolute minimization function of eq 24. As discussed elsewhere,[10] effective internal correlation times for spins with high order parameters usually cannot be determined precisely from natural abundance ^{13}C relaxation investigations; consequently, internal correlation times have not been reported for the aromatic spins. Results for the aromatic spins obtained by minimizing the relative minimization function of eq 25 were statistically indistinguishable from the results in Table IV and have not been reported. Values of the parameters for the Lipari–

(53) Kay, L. E.; Bull, T. E.; Nicholson, L. K.; Griesinger, C.; Schwalbe, H.; Bax, A.; Torchia, D. A. *J. Magn. Reson.* **1993**, *100*, 538–558.

Table V. Model-Free Parameters for Methyl ^{13}C Spins in Xfin-31 by Absolute Minimization[a]

nucleus	S^2	τ_e (ps)	R_a (s^{-1})	S_0^2	χ_r^2
Leu 5 δ_a	0.044 ± 0.003	12 ± 1	0.10 ± 0.01	0.40 ± 0.03	5.7
Leu 5 δ_b	0.062 ± 0.004	22 ± 1	0.49 ± 0.03	0.56 ± 0.04	1.6
Val 11 γ_a	0.063 ± 0.004	16 ± 1		0.57 ± 0.04	0.9
Val 11 γ_b	0.091 ± 0.006	21 ± 1		0.82 ± 0.05	10.0
Ala 15 β	0.160 ± 0.010	44 ± 2		1.44 ± 0.09	1.8
Leu 16 δ_1	0.127 ± 0.008	28 ± 2		1.14 ± 0.07	13.5
Leu 16 δ_2	0.093 ± 0.006	18 ± 1		0.84 ± 0.05	4.7
Val 22 γ_a	0.069 ± 0.004	13 ± 1	0.54 ± 0.04	0.62 ± 0.04	4.8
Val 22 γ_b	0.086 ± 0.006	23 ± 1	0.21 ± 0.01	0.78 ± 0.05	4.0

[a] Shown arer the order parameters and exchange contributions to the phenomenological R_2 calculated from the relaxation data of Table III using eqs 1–5 and 16. Parameters were determined by using the absolute minimization function (eq 24). The overall rotational correlation time was determined to be 1.6 ± 0.1 ns (at 303 K in D_2O). Also given are the values of the order parameter for the symmetry axis of the methyl group, S_0^2, calculated using eq 19.

Table VI. Model-Free Parameters for Methyl ^{13}C Spins in Xfin-31 by Relative Minimization[a]

nucleus	S^2	τ_e (ps)	R_a (s^{-1})	S_0^2	χ_r^2
Leu 5 δ_a	0.043 ± 0.003	12 ± 1	0.08 ± 0.01	0.39 ± 0.03	0.01
Leu 5 δ_b	0.056 ± 0.003	22 ± 1	0.47 ± 0.04	0.50 ± 0.04	0.01
Val 11 γ_a	0.060 ± 0.004	17 ± 1		0.54 ± 0.04	0.01
Val 11 γ_b	0.078 ± 0.005	23 ± 1		0.70 ± 0.05	0.02
Ala 15 β	0.160 ± 0.010	44 ± 3		1.44 ± 0.09	0.01
Leu 16 δ_1	0.126 ± 0.007	27 ± 2		1.14 ± 0.07	0.06
Leu 16 δ_2	0.088 ± 0.006	18 ± 1		0.79 ± 0.05	0.01
Val 22 γ_a	0.083 ± 0.005	12 ± 1	0.37 ± 0.02	0.75 ± 0.04	0.01
Val 22 γ_b	0.075 ± 0.005	24 ± 1	0.21 ± 0.01	0.68 ± 0.05	0.01

[a] Shown are the order parameters and exchange contributions to the phenomenological R_2 calculated from the relaxation data of Table III using eqs 1–5 and 16. Parameters were determined by using the relative minimization function (eq 25). The overall rotational correlation time was determined to be 1.8 ± 0.1 ns (at 303 K in D_2O). Also given are the values of the order parameter for the symmetry axis of the methyl group, S_0^2, calculated using eq 19.

Szabo model-free formalism for the methyl ^{13}C spins were calculated from the data of Table III using eqs 1–5 and 16. Results for the methyl spins obtained by minimizing eqs 24 and 25 are reported in Tables V and VI, respectively. Model-free parameters calculated by minimizing eqs 24 and 25 are indistinguishable statistically for Leu 5, Leu 16, and Ala 15. The order parameter for Val 11 γ_b is somewhat smaller when eq 25 is minimized. Order parameters for Val 22 γ_a and γ_b are significantly different when eq 24 is used, but the two order parameters are indistinguishable when eq 25 is used as the minimization function. Values of the symmetry-axis order parameter, S_0^2, calculated using eq 19, have been included in Tables V and VI for the methyl spins. The optimized values of R_a for Leu 5 and Val 22 are less than twice the uncertainties in the measured values of R_2 and have not been analyzed further. High-resolution solution structure determination shows that the Val 22 side chain is conformationally disordered about χ_1 (Lee, M. S.; Mortishire-Smith, R. J.; Wright, P. E. Unpublished results), which may be responsible for exchange

Table VII. Relaxation Parameters for Diffusion Model for Methyl ^{13}C Spins in Xfin-31[a]

nucleus	S_0^2	τ_0 (ps)	τ_c (ps)	R_a (s^{-1})	χ_i^2
Leu 5 δ_a	0.40 ± 0.03	26 ± 2	28 ± 2	0.07 ± 0.01	5.0
Leu 5 δ_b	0.56 ± 0.04	94 ± 7	40 ± 3	0.45 ± 0.04	2.7
Val 11 γ_a	0.56 ± 0.04	53 ± 6	32 ± 2		1.0
Val 11 γ_b	0.38 ± 0.04	1000 ± 60	35 ± 3		0.1
Ala 15 β	1.0		107 ± 8		44.3
Leu 16 δ_1	1.0		61 ± 6		18.8
Leu 16 δ_2	0.83 ± 0.07	137 ± 11	32 ± 3		4.1
Val 22 γ_a	0.64 ± 0.05	13 ± 1	32 ± 2	0.49 ± 0.04	4.2
Val 22 γ_b	0.78 ± 0.06	0	65 ± 5	0.15 ± 0.01	5.3

[a] Shown are the symmetry axis order parameters and effective correlation times, the characteristic diffusion time for methyl rotation, and exchange contributions to the phenomenological R_2 calculated from the relaxation data of Table III using eqs 1–5 and the restricted rotational diffusion model for methyl rotation (eq 18 with $a = b$). Parameters were determined by minimizing eq 24. Values of S_0^2 for Ala 15 β and Leu 16 δ_1 were fixed at 1.0. The overall rotational correlation time was determined to be 1.7 ± 0.1 ns (at 303 K in D_2O).

contributions to R_2 for this residue. The minimum value of χ_i^2 (eqs 24 and 25) measures the degree of fit between the experimental data and the analytical model for the ith spin;[10] in the present cases, the values of χ_i^2 calculated from eq 24 generally are <6, although values >10 are obtained for Tyr 1 δ, Phe 10 ϵ, Val 11 γ_b, and Leu 16 δ_1. For those residues for which R_a was included in the analysis, the values of χ_i^2 are reduced by a factor of ≥5, compared to analysis with $R_a = 0$; however, the values of the order parameters and internal correlation times are not changed substantially. The observed ranges for χ_i^2 are consistent with results obtained in previous investigations.[10,16,19] Values of χ_i^2 calculated using eq 25 are <0.1, which indicates that the model-free analysis reproduces the experimental relaxation parameters to within a relative root-mean-square deviation of <10%. Comparisons of the values of χ_i^2 calculated from eqs 24 and 25 are not meaningful. Model-free parameters were also determined for the methyl spins using only the R_1 and η data from Table III; the results for the order parameters and internal correlation times are not statistically different from the data presented in Table V. Extending eq 16 to include contributions from internal motions on a second time scale[54] or anisotropic overall rotational motion[41] did not significantly improve the fit between the theoretical models and the experimental data.

The relaxation parameters for the methyl ^{13}C spins in Table III also were analyzed using specific descriptions of the internal motions of the methyl group to explicitly separate rotational motions of the methyl group from motions of the methyl symmetry axis. Results for the analysis using the diffusion model for methyl rotation (eq 18 with $a = b$) and the absolute minimization function given by eq 24 are presented in Table VII. Results using the jump model for methyl rotation (eq 18 with $a = 1$) are similar to the results presented in Table VII and are not shown. Except for Ala 15 C^β, the values of χ_i^2 obtained for analyses based on eq 18 and the model-free formalism (eq 16) are similar. Except for Val 11 γ_b, the symmetry-axis order parameters determined from eq 18 and from the model-free formalism using eqs 16 and 19 are similar. Effective correlation times for symmetry-axis motions are <150 ps, except for Val 11 γ_b. Characteristic times for methyl rotation are rapid (<75 ps) for all spins except Ala 15 C^β.

Typical time-resolved fluorescence depolarization data for Tyr 1 are shown in Figure 5 for zinc-complexed Xfin-31 and in Figure 6 for the zinc-free peptide. Fluorescence lifetime and anisotropy parameters determined simultaneously using eqs 26–29 are given in Tables VIII and IX: results obtained with sampling intervals of 9.55 and 35.91 ps/channel were averaged by using the squares of the uncertainties in the parameters as weighting functions.

(54) Clore, G. M.; Szabo, A.; Bax, A.; Kay, L. E.; Driscoll, P. C.; Gronenborn, A. M. *J. Am. Chem. Soc.* **1990**, *112*, 4989–4991.

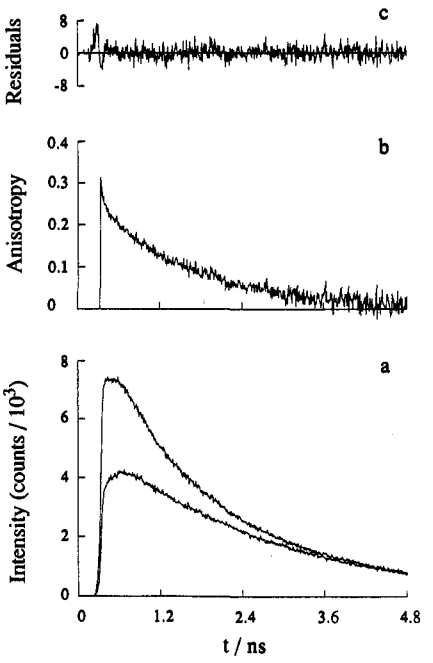

Figure 5. Time-resolved fluorescence depolarization of Tyr 1 in zinc-complexed Xfin-31. Shown in part a are the polarized fluorescence intensities, $I_\parallel(t)$ (upper curve) and $I_\perp(t)$ (lower curve). The time-dependent fluorescence anisotropy is shown in part b. The weighted deviations between the experimental and best-fit difference curves, $I_\parallel(t) - I_\perp(t)$, are shown in part c.

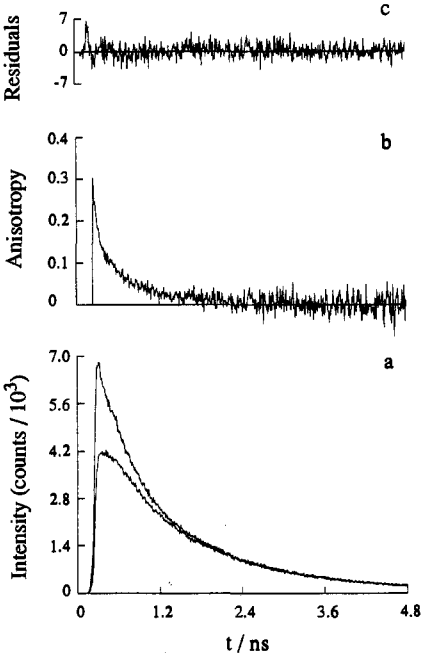

Figure 6. Time-resolved fluorescence depolarization of Tyr 1 in zinc-free Xfin-31. Shown in part a are the polarized fluorescence intensities, $I_\parallel(t)$ (upper curve) and $I_\perp(t)$ (lower curve). The time-dependent fluorescence anisotropy is shown in part b. The weighted deviations between the experimental and best-fit difference curves, $I_\parallel(t) - I_\perp(t)$, are shown in part c.

Two lifetime components and two anisotropy components are necessary to fit the depolarization data for the zinc-complexed peptide; three lifetime components and two anisotropy components are required for the zinc-free peptide. Average values of the reduced χ^2 obtained from the nonlinear least squares fits are approximately 1.2–1.4; the quality of the fits are not improved statistically by including additional lifetime or anisotropy components. As shown in Figures 5c and 6c, systematic trends are

Table VIII. Fluorescence Lifetime Parameters for Tyr 1 of Xfin-31[a]

form	T (K)	τ_1 (ns)	τ_2 (ns)	α_1	α_2	α_3
Zn	283	0.97 ± 0.34	2.63 ± 0.06	0.09 ± 0.04	0.91	
Zn	293	0.75 ± 0.26	2.28 ± 0.06	0.10 ± 0.04	0.90	
Zn	303	1.05 ± 0.25	2.03 ± 0.06	0.12 ± 0.06	0.88	
apo[b]	293	0.22 ± 0.09	0.54 ± 0.13	0.16 ± 0.07	0.39 ± 0.04	0.45

[a] As described in the text, lifetime and anisotropy decay parameters were determined simultaneously using eqs 26–29. Anisotropy parameters and χ_r^2 values are given in Table IX. [b] τ_3 = 1.73 ± 0.09 ns.

Table IX. Anisotropy Decay Parameters for Tyr 1 of Xfin-31[a]

form	T (K)	τ_{r1} (ns)	τ_{r2} (ps)	r_{01}	r_{02}	χ_r^2
Zn	283	2.00 ± 0.10	28 ± 19	0.24 ± 0.01	0.11 ± 0.04	1.35
Zn	293	1.42 ± 0.09	35 ± 29	0.23 ± 0.01	0.08 ± 0.04	1.38
Zn	303	1.09 ± 0.07	36 ± 25	0.22 ± 0.01	0.10 ± 0.03	1.24
apo	293	0.59 ± 0.13	47 ± 23	0.13 ± 0.02	0.18 ± 0.04	1.25

[a] As described in the text, lifetime and anisotropy decay parameters were determined simultaneously using eqs 26–29. Lifetime parameter values are given in Table VIII.

Table X. Model-Free Parameters for Tyr 1 in Xfin-31 from Fluorescence Depolarization[a]

form	T (K)	τ_m (ns)	S^2	τ_e (ps)
Zn	283	2.00 ± 0.10	0.68 ± 0.08	28 ± 18
Zn	293	1.42 ± 0.09	0.73 ± 0.09	34 ± 27
Zn	303	1.09 ± 0.07	0.69 ± 0.08	34 ± 24
apo	293	0.59 ± 0.13	0.42 ± 0.10	44 ± 20

[a] Model-free parameters determined from the data in Table IX using eqs 32 and 33. The overall rotational correlation times for the zinc complex of Xfin-31 are a linear function of η_w/T, in which η_w is the viscosity of H_2O, with a correlation coefficient of 0.999. For comparison with the values of τ_m determined by fluorescence spectroscopy in H_2O solution, the values determined from NMR relaxation measurements in D_2O must be reduced by approximately 22% to account for the differences in viscosity of D_2O and H_2O.

not observed in the residuals from the curve fitting. The average value of the limiting polarization anisotropy was 0.32 ± 0.01 and is in good agreement with reported values for Tyr.[22] Values of the parameters for the Lipari–Szabo model-free formalism for the emission dipole of Tyr 1 calculated from the data of Table IX using eqs 32 and 33 are given in Table X. As shown, the values of S^2 and τ_e for the zinc-complexed peptide are independent of the temperature of the sample, within experimental uncertainties, while τ_m varies linearly with the ratio of the viscosity and temperature as predicted by the Stokes–Einstein equation.[55] The order parameter and overall rotational correlation time are substantially smaller for the unfolded zinc-free peptide.

Discussion

Accurate characterization of internal motional properties of proteins requires that the experimental NMR techniques used to measure spin relaxation parameters be designated to minimize effects not incorporated into the above theoretical formalism. In addition to the well-known effects of ^1H–^{13}C dipolar cross-relaxation on ^{13}C spin relaxation,[56,57] other investigations have emphasized potentially significant errors that can arise due to evolution of heteronuclear scalar coupling during the spin–echo period of CPMG experiments,[58–60] cross-correlation between dipolar and CSA relaxation mechanisms,[59,60] creation of multiple-spin operators during polarization-transfer schemes for methyl groups,[46,50,53] and cross-correlation between C–H vectors in methyl groups.[50,53] In the present study, such effects are minimized by using short spin–echo delays in the CPMG experiments,[50,60] proton decoupling in inversion–recovery and CPMG experiments for aromatic carbon spins,[50,60,61] and magic angle editing pulses in polarization transfers for methyl carbon spins.[46]

The relaxation parameters for methyl and protonated aromatic carbon spins are analyzed using a model-free formalism and explicit descriptions of molecular motions. Equations 1–3 comprise an overdetermined nonlinear system of equations for the parameters of the auto-spectral density function of each C–H vector (eqs 16 and 18) with coefficients, given by the relaxation parameters, that are corrupted by observational noise. Determining the roots of this system of equations is mathematically intractable;[48] therefore, the problem is converted into a least squares minimization by construction of an approximate χ^2 error function (eqs 24 and 25). Because the optimal choice of the form of the error function is unknown, the relaxation data have been analyzed using two different error functions. The absolute minimization function eq 24) depends upon the experimental uncertainties in the relaxation parameters; the relative minimization function (eq 25) is independent of the experimental uncertainties. In most cases, the optimized parameters of the auto-spectral density functions determined using eqs 24 and 25 were statistically indistinguishable; however, for some spins, particularly Val 22 γ_a and γ_b, the results differ significantly depending on the choice of error function. Thus, comparison of the results obtained with alternative forms of the error function is an important test of the stability of the optimized motional parameters. The present results, together with the results of the previous investigation of the motional properties of aliphatic C–H groups,[10] provide a description of the intramolecular dynamics of all protonated, non-methylene, carbon spins in the peptide.

The structure of Xfin-31[62] consists of an antiparallel β hairpin that extends from Tyr 1 to Phe 10, a loop from Phe 10 to Lys 13, and a helix that extends from Lys 13 to Lys 24. The zinc ion is ligated to two Cys residues in the β hairpin and two His residues in the helix. Previous investigation[10] of backbone C^α spins indicated that (1) the C^α residues in elements of secondary structure (the antiparallel β hairpin and the helix) have high order parameters (≈0.87); (2) the N-terminal Tyr has a slightly lower order parameter of 0.75; (3) order parameters decrease rapidly at the C-terminus to a value of 0.30 for Asn 25, which suggests that the terminus is disordered; (4) the loop region has lower order parameters (≈0.79) than the secondary structural elements; and (5) a conformational-exchange process occurs in the zinc-binding site. Results for a small number of side chain methine ^{13}C spins indicated that the order parameters decreased as the distance from the backbone increased. Previously measured values of the model-free order parameters for methine carbons of the aromatic residues (His, Phe, and Tyr) and for the Ala, Leu, and Val residues are given in Table XI[10] to facilitate comparison with the aromatic and methyl carbon order parameters determined in the present work.

Order parameters for Tyr and the two His aromatic carbon spins are similar to order parameters for the backbone C^α spins of the same residues (Table XI), which suggests that these aromatic side chains have little additional motional freedom relative to the peptide backbone on picosecond to nanosecond time scales. For Phe 10, order parameters for the C^δ and C^α spins are similar and order parameters for C^ϵ and C^ζ spins are somewhat larger; thus, the C^ζ end of the Phe 10 phenyl ring is more conformationall restricted than the backbone of the peptide. In addition, the similar order parameters obtained for the C^ϵ and C^ζ spins and the differences in order parameters observed for the

(55) Cantor, R. C.; Schimmel, P. R. *Biophysical Chemistry*; W. H. Freeman: San Francisco, CA, 1980; Vol. II.
(56) Solomon, I. *Phys. Rev.* **1955**, *99*, 559–565.
(57) Dellwo, M. J.; Wand, A. J. *J. Magn. Reson.* **1991**, *91*, 505–516.
(58) Peng, J. W.; Thanabal, V.; Wagner, G. *J. Magn. Reson.* **1991**, *95*, 421–427.
(59) Kay, L. E.; Nicholson, L. K.; Delagio, F.; Bax, A.; Torchia, D. A. *J. Magn. Reson.* **1992**, *97*, 359–375.
(60) Palmer, A. G.; Skelton, N. J.; Chazin, W. J.; Wright, P. E.; Rance, M. *Molec. Phys.* **1992**, *75*, 699–711.
(61) Boyd, J.; Hommel, U.; Campbell, I. D. *Chem. Phys. Lett.* **1990**, *175*, 477–482.
(62) Lee, M. S.; Gippert, G. P.; Soman, K. V.; Case, D. A.; Wright, P. E. *Science* **1989**, *245*, 635–637.

Table XI. Model-Free Parameters for Methine ^{13}C Spins in Xfin-31[a]

nucleus	S^2	τ_e (ps)
Tyr 1 α	0.75 ± 0.04	52 ± 34
Leu 5 α	0.88 ± 0.05	
Leu 5 γ	0.48 ± 0.03	26 ± 9
Phe 10 α	0.74 ± 0.03	14 ± 12
Val 11 α	0.81 ± 0.03	16 ± 22
Val 11 β	0.63 ± 0.03	36 ± 11
Ala 15 α	0.86 ± 0.04	60 ± 140
Leu 16 α	0.88 ± 0.04	
His 19 α	0.88 ± 0.04	
Val 22 α	0.78 ± 0.04	51 ± 45
Val 22 β	0.55 ± 0.05	54 ± 16
His 23 α	0.74 ± 0.06	17 ± 22

[a] Model-free results for the methine C–H bond vectors of Ala, His, Leu, Phe, Tyr, and Val residues. Results are taken from Table III of Palmer et al.[10] Model-free parameters were not reported for Leu 16 γ.

C^δ and C^ϵ spins suggest that motion about the C^γ–C^ζ axis of the phenyl ring is very limited and lacks axial symmetry; otherwise, eq 14 predicts that the order parameters would have the relationship $C^\zeta > C^\epsilon \approx C^\delta$. The high order parameters observed for the aromatic spins of Phe 10 and for the symmetry axes of the methyl groups of Leu 16 (see below) are consistent with the close contacts observed between these two side chains in the NMR structure of the peptide and support the conclusion that these side chains form a small but stable hydrophobic core.[62] However, since only single resonances are observed for the δ and ϵ spins of Phe 10 (Figure 2a), movements of the phenyl ring or the Leu side chain must occur to permit flipping of the aromatic ring on a time scale that is slow compared with rotational motion but fast compared with the chemical shift differences between the symmetry-related spins. The very large values of R_a obtained for the His residues supports the previous conclusion that a chemical-exchange process occurs in the zinc-binding site. Interestingly, only one of the two protonated ^{13}C spins for each His is affected by exchange broadening, and the affected spin is different for the two His residues; consequently, the chemical shift difference between conformers must be large only for one of the protonated carbon nuclei on each ring. Since R_a is only appreciable if $k\tau > 1$, the rate constant for chemical exchange is >2000 s^{-1}.

Because chemical shift tensors have not been measured experimentally for the protonated aromatic carbon spins in amino acids, the values of $\Delta\sigma$ (Table I) used in eq 5 were estimated from results for other aromatic molecules and from theoretical calculations.[63-65] The values of σ_{22} and σ_{33} in Table I are not equal, and the theoretical descriptions appropriate for an axially symmetric shift tensor are not strictly applicable. In addition, the principal axis of the chemical shift tensor for ^{13}C spins in aromatic moieties is oriented approximately perpendicular to the plane of the aromatic ring[65] ($\beta_{DF} = 90°$ for Tyr and Phe); thus, the autocorrelation functions for the dipolar and CSA relaxation mechanisms are not necessarily equal (eq 13). However, since $C^2/D^2 \approx 0.2$ (eqs 4 and 5), relaxation is dominated by the dipolar interaction, and complications arising from the description of the CSA relaxation do not dramatically affect the given results. Altering $\Delta\sigma$ for an aromatic spin by ~20 ppm changes the order parameter by ~0.05, which is comparable to the reported uncertainties in the order parameters (Table IV). Consequently, the conclusions derived from comparison of the order parameters for the aromatic spins do not depend upon the exact values chosen for $\Delta\sigma$; nonetheless, more detailed interpretation of small differences in order parameters for aromatic spins awaits more complete measurements of chemical shift anisotropies for aromatic amino acids.

As a consequence of internal rotation of the methyl group, order parameters for methyl ^{13}C spins are approximately an order of magnitude smaller than order parameters for backbone C^α spins and effective correlation times are in the range 10–25 ps, with the exception of the correlation time for Ala 15 C^β (Tables V and VI). In accordance with results obtained previously for the side chain methine carbon spins (Table XI), the order parameters for the methyl groups generally are smaller for residues with longer side chains. The symmetry-axis order parameters for Leu 16 C^δ spins are approximately unity and, as discussed above, reflect the packing of the side chains of Phe 10 and Leu 16 in the hydrophobic core of the molecule. As shown by comparison of Tables V and VI with Table XI, Leu and Val residues can be classified according to the relationships between the symmetry-axis order parameters for the geminal methyl spins and the order parameters for side chain methine spins. For example, all three order parameters for Leu 5 agree statistically; in contrast, for Val 11, the symmetry-axis order parameter for the γ_a methyl agrees well with the order parameter for the C^β spin, and the order parameter for γ_b is significantly larger. The results for Val 22 depend upon the choice of error function; however, either one (Table V) or both (Table VI) of the methyl symmetry-axis order parameters are larger than the methine C^β order parameter. Similarly, the two symmetry-axis order parameters for Leu 16 are significantly different, although the C^γ methine order parameter is unknown. The symmetry-axis order parameter for Ala 15 C^β is larger than the theoretical maximum value, which suggests that, for this residue at least, eq 19 is not applicable.

The observed differences between the order parameters for geminal methyl carbons of Leu and Val residues or the anomalous order parameter for Ala 15 C^β cannot be attributed to distortions of ideal tetrahedral geometry of the methyl group. Neutron diffraction studies of crystalline Ala and Val[66,67] indicate that the angle between the symmetry axis and the C–H bond vectors is decreased by 1–3° and that relative distortions between geminal methyl groups are <1° in Val. Thus, the reported symmetry axis order parameters calculated from eq 19 may be underestimated by ~20%; however, relative differences between order parameters for geminal methyl groups are much less affected by distortions of the methyl geometry. Incidentally, if $\beta = 68.5°$ is used rather than 70.5° in eq 19, the methyl symmetry-axis order parameter for the Leu 16 δ_1 methyl group, as well as for Ala 15 C^β, is significantly greater than unity.

Alternatively, if internal motions of the methyl groups are not close to the extreme narrowing limit, then values of the order parameters are overestimated by the model-free analysis.[34] In particular, the order parameter for the symmetry axis of a methyl group may be overestimated by eq 19 if steric interactions increase the barriers to internal rotation of the methyl group. In the present case, the model-free formalism is expected to be an accurate description for internal motions with $\omega\tau_e < 0.3$, which implies $\tau_e < 75$ ps.[34] The effective correlation times determined from the model-free analysis were <75 ps for all of the methyl groups (Tables V and VI); additionally, as shown in Table VII, the correlation times for internal rotation were <75 ps for the methyl groups of Val and Leu. Thus, slow internal rotations of methyl groups do not appear to be the cause of the observed differences between the order parameters for geminal methyl carbons of Leu and Val residues. In contrast, the methyl symmetry-axis order parameter for Ala 15 calculated for the model-free analysis is larger than unity, and the relaxation data was not reproduced well by use of either the diffusion or jump models for methyl

(63) Moore, A. C. Ph.D. Thesis, University of California, Berkeley, CA, 1976.
(64) Prado, F. R.; Giessner-Prettre, C. *J. Magn. Reson.* **1982**, *47*, 103–117.
(65) Veeman, W. S. *Prog. Nucl. Magn. Reson. Spectrosc.* **1984**, *16*, 193–235.
(66) Lehmann, M. S.; Koetzle, T. F.; Hamilton, W. C. *J. Am. Chem. Soc.* **1972**, *94*, 2657–2660.
(67) Koetzle, T. F.; Golic, L.; Lehmann, M. S.; Verbist, J. J.; Hamilton, W. C. *J. Chem. Phys.* **1974**, *60*, 4690–4696.

rotation. In solid samples, correlation times for methyl rotation of 1.3 ns have been measured for Ala by solid-state NMR spectroscopy; the corresponding correlation times for Val and Leu are <200 ps.[68] Consequently, slow rotational motions of the methyl group may provide an explanation of the anomalous results for Ala 15.

The simplest explanation of the observed differences in order parameters of the geminal methyl and methine spins is provided by eq 14: if the order parameters for geminal methyl symmetry axes and the side chain methine carbon spins are different, then the distributions of conformational states accessible to the methyl symmetry axes and the methine bond vector do not have three-fold or higher rotational symmetry. Thus, for Leu 5, the joint equilibrium distribution for the χ_2 dihedral angle and the orientation of the C^β–C^γ axis have at least three-fold symmetry. If the χ_2 dihedral angle and the orientation of the C^β–C^γ axis are independent, then either the equilibrium distribution of the χ_2 dihedral angle or the orientation of the C^β–C^γ axis is at least three-fold symmetric. For Val 11, Leu 16, and Val 22, the order parameters for the methyl symmetry axes and the methine C–H vectors are not rotationally averaged and particular bond vectors are evidently more highly constrained sterically than other vectors. For example, the order parameters for Leu 16 indicate that the distributions of the χ_2 dihedral angle and of the C^β–C^γ axis are not symmetric and that the δ_1 methyl group is more highly constricted than the δ_2 methyl; in support of this result, NOESY data and the solution structure for Xfin-31 indicate that the Leu 16 δ_1 methyl group has a larger number of relatively short-range (<3.5 Å) interactions with the side chains of Phe 10 and Gln 20 than does the Leu 16 δ_2 methyl. Although the lack of stereospecific assignments for the other geminal methyl groups hinder detailed analysis, the present results suggest that order parameters for geminal methyl groups and side chain methine spins are sensitive probes for local differences in steric constraints to side chain mobility.

Pioneering studies of ^{13}C relaxation in proteins were performed over a dozen years ago for bovine pancreatic trypsin inhibitor[69] and sperm whale myoglobin.[70,71] The relaxation parameters originally were analyzed using spectral density functions derived from the diffusion-in-a-cone model; however, Lipari and Szabo subsequently reanalyzed the data using the model-free formalism.[41] The general conclusions drawn from these early studies are corroborated by the present results. In particular, the aromatic rings in the trypsin inhibitor did not have significantly greater mobilities than the protein backbone on picosecond to nanosecond time scales, and methyl rotation was superimposed upon side chain motions with considerable amplitudes for both trypsin inhibitor and myoglobin. More recently, order parameters and effective correlation times have been reported for a number of ^{13}C spins in cyclosporin A[9] and for the geminal methyl groups of 11 Leu residues in liganded and unliganded forms of *Staphylococcal nuclease*.[12] In accordance with the present results, the order parameters obtained for the methyl symmetry axes of cyclosporin A were larger than the order parameters for the corresponding methine vectors in *N*-methylleucine, valine, and *N*-methylvaline residues. The methyl symmetry-axis order parameters range from 0.34 to 0.92 in *S. nuclease*, which is similar to the range observed for Leu 5 and Leu 16 in Xfin-31. The differences between the order parameters for geminal methyl carbon spins in *S. nuclease* generally are smaller than those in Xfin-31; however, large differences are observed in some cases (e.g. Leu 38 in unliganded *S. nuclease*). Order parameters have not been reported for the methine C^γ vectors in *S. nuclease*; consequently, comparisons between the order parameters for the methyl symmetry axes and the methine bond vectors are not possible.

As the body of results probing internal dynamics of proteins by NMR spectroscopy becomes larger, comparisons with results from other techniques become increasingly important for assessing the accuracy and generality of the results. The absence of Trp residues in Xfin-31 has permitted comparison of motional parameters for Tyr 1 to be determined by fluorescence spectroscopy as well as NMR spectroscopy. In principle, the order parameters measured by the two techniques depend upon the relative orientations of the tyrosyl emission dipole and the C–H vectors, as indicated by eq 13, and are not necessarily equivalent. Nonetheless, as shown by comparison of Tables IV and X, the order parameters for the Tyr ring in the folded zinc finger determined by the two techniques are statistically indistinguishable. The higher sensitivity of fluorescence spectroscopy, compared with natural abundance ^{13}C NMR spectroscopy, enables the internal correlation time for the Tyr ring to be determined with greater accuracy. Within statistical limitations, the order parameters and effective correlation times for the emission dipole are independent of temperature over the range 283–303 K. This result suggests that the observed motions represent fluctuations within a single potential minimum in the conformational space of the aromatic ring, rather than transitions over an activation barrier. Another advantage of the fluorescence decay experiments is that both the native (folded) and zinc-free (unfolded) forms of the peptide have been studied. In the absence of zinc, both the order parameter and apparent overall rotational correlation time are dramatically reduced compared with the results obtained in the presence of zinc. The differences between the motional parameters of the peptide in the presence and absence of zinc mirror changes in NMR chemical shift dispersions reported previously[45] and suggest that, in the absence of zinc, the decay of anisotropy is dominated by relatively rapid, large-amplitude, local motions of the disordered peptide.

Accounting for the differences in the viscosity of H_2O (0.798 cp) and D_2O (0.969 cp) at 303 K, the overall rotational correlation time determined from the NMR results for backbone, aromatic, and methyl spins is 1.36 ± 0.07 ns in H_2O and is significantly larger than the fluorescence result of 1.09 ± 0.01 ns. A similar observation has been made for calbindin D_{9k}, in which a rotational correlation time of 4.25 ± 0.04 ns was obtained from ^{15}N NMR relaxation measurements[16] and 3.29 ± 0.08 ns was obtained by fluorescence spectroscopy (Carlström, G.; Chazin, W. J.; Millar, D. P. Unpublished results). Calculation of the rotational correlation time for Xfin-31 at 303 K from the Stokes–Einstein equation, using 0.35 g of H_2O/1 g of peptide as an estimate of hydration of the molecule, gives τ_m = 1.0 ns; assuming a 3-Å hydration layer surrounding the peptide yields τ_m = 1.5 ns. Thus, both the NMR and fluorescence results are consistent with theoretical estimates of 1.0–1.5 ns for the overall rotational correlation time. The principal components of the inertia tensor calculated from the NMR solution structure of Xfin-31 are 1.00: 1.43:1.84. Shape-factor corrections[55] to the Stokes–Einstein correlation time do not exceed 15%, regardless of the orientation of the emission dipole of the Tyr relative to the principal axes of Xfin-31. At present, the question of whether the rotational correlation time is overestimated by the NMR results, perhaps due to contributions of other relaxation mechanisms not considered in eqs 1–3 or due to slight aggregation at the higher concentrations used for NMR spectroscopy, or underestimated by the fluorescence result cannot be resolved.

(68) Torchia, D. A. *Annu. Rev. Biophys. Bioeng.* **1984**, *13*, 125–144.
(69) Richarz, R.; Nagayama, K.; Wüthrich, K. *Biochemistry* **1980**, *19*, 5189–5196.
(70) Jones, W. C.; Rothgeb, T. M.; Gurd, F. R. N. *J. Biol. Chem.* **1976**, *251*, 7452–7460.
(71) Wittebort, R. J.; Rothgeb, T. M.; Szabo, A.; Gurd, F. R. N. *Proc. Natl. Acad. Sci. U.S.A.* **1979**, *76*, 1059–1063.
(72) Müller, L.; Ernst, R. R. *Mol. Phys.* **1979**, *38*, 963–992.
(73) States, D. J.; Habekorn, R. A.; Ruben, D. J. *J. Magn. Reson.* **1982**, *48*, 286–292.

Conclusion

Proton-detected ^{13}C NMR spectroscopy has been used to measure spin–lattice and spin–spin relaxation rate constants and the steady-state $\{^1H\}$–^{13}C NOE for the protonated aromatic carbon spins and for the methyl carbon spins in the zinc-finger peptide Xfin-31; in addition, time-resolved fluorescence spectroscopy has been used to measure independently the polarization anisotropy decay of the Tyr fluorophore in the peptide in the presence and absence of zinc. The relaxation and depolarization results were analyzed using a model-free formalism and explicit motional models to describe internal motions of the C–H bond vectors in the peptide. Internal motional parameters for the tyrosine ring measured by NMR and fluorescence spectroscopies are in good agreement. Order parameters for aromatic moieties are large and are consistent with previously determined structural features of the peptide. Spin–spin relaxation rate constants for His residues indicate that a chemical-exchange process occurs in the zinc-binding site of the peptide. Model-free order parameters for methyl groups indicate that longer side chains generally have more conformational freedom; although, in particular cases, local packing effects can highly restrict the side chains of even Leu residues. In some cases, particularly for Ala 15, relaxation may be mediated by motions outside the extreme narrowing limit. Comparisons between order parameters for side chain methine and methyl groups in Leu and Val residues demonstrate that, in some instances, the steric constraints to internal motions of the side chain are anisotropic and the internal motions lack rotational symmetry. The results complement and extend the characterization of backbone dynamics previously reported for Xfin-31 and indicate the considerable potential for investigations of dynamic processes in biomolecules by NMR and fluorescence spectroscopies.

Acknowledgment. This work was supported by grants from the National Institutes of Health [GM 40089 (M.R.), GM 44060 (D.P.M.) and GM 36643 (P.E.W.)]. A.G.P. was supported by a National Science Foundation Postdoctoral Fellowship in Chemistry awarded in 1989 (CHE 8907510). We thank L. E. Kay and A. Bax for providing a preprint of ref 12.